COO-2421-04

MASTER

Corrosion, Stress Corrosion Cracking, and Electrochemistry of the Iron and Nickel Base Alloys in Caustic Environments

R. W. Staehle
Professor

A. K. Agrawal
Adjunct Assistant Professor

Department of Metallurgical Engineering
The Ohio State University
Columbus, Ohio

Progress Report for the Period
1 Mar. 1977 to 28 February 1978

United States
Energy Research and Development Administration

Contract No. EY-76-S-02-2421. *000

EB

DISCLAIMER

TABLE OF CONTENTS

1.0 ABSTRACT

The straining electrode technique was used to evaluate the stress corrosion cracking (SCC) susceptibility of AISI 304 stainless steel in 20N NaOH solution, and of Inconel 600 Alloy and Incoloy 800 Alloy in boiling 17.5N NaOH solution. The crack propagation rate estimated from the straining experiments correlated well with the previous constant load experiments. It was found that the straining electrode technique is a useful method for estimating, through short term experiments, parameters like crack propagation rate, crack morphology, and repassivation rate, as a function of the electrode potential. The role of alloying elements on the crack propagation rate in the above alloys are also discussed.

Type 304 stainless steel was tested for its resistance to SCC in boiling 20N NaOH solution in the presence of sixteen different additives. It was found that potential of Type 304 in the solution is the dominant factor in promoting or inhibiting SCC of the alloy. The anodic kinetics of the alloy in the caustic solution is not affected by the foreign ions introduced from the various additives, the kinetics is controlled largely by the OH^- ions in the solution and the potential. In a concentrated caustic solution like 20N NaOH the predominance of OH^- ions overwhelms the effect of other anions, even if these anions, e.g., $SO_4^=$, PO_4^{-3}, and $MoO_4^=$, etc. are present in saturated concentrations. The additives which form a redox couple, e.g., $CrO_4^=/CrO_3^=$, whose equilibrium potential in the caustic solution falls in the passive region of Type 304 promote passivation and these are effective as SCC inhibitors.

Controlled potential long term coulometric experiments with pure nickel have been done in 10N NaOH at 110°C and in 17.5N NaOH at 130°C.

Passivation of nickel in caustic solutions occurs after an incubation time which is dependent upon the applied potential. The incubation time is the time required for the nickel ions at the metal-solution interface to reach saturation concentration, whereupon oxide (hydroxide) precipitation occurs. The film growth after incubation follows a logarithmic kinetics. The dissolution-precipitation model of Bockris et al for Ni in acid solutions appears to be also applicable to caustic solutions.

Potentiodynamic polarization curves of pure iron have been established in sulfate solutions at pH values of 0.5 to 13, temperatures of 25 to 85°C, and sulfide ion concentrations of 0 to 300 ppm. The anodic kinetics of iron increased in both the active and the passive regions in the presence of sulfide in the solutions. The critical potential for passivation also increased with increasing sulfide concentration in the solutions. In acid solutions the passive region showed unstability with pitting tendency due to sulfide, whereas no such pitting tendency was observed in basic solutions.

2.0 INTRODUCTION

The work accomplished in the project "Corrosion, Stress Corrosion Cracking, and Electrochemistry of the Iron and Nickel Base Alloys in Caustic Environments" during the current reporting period of 1 March 1977 to 28 February 1978 is presented herein. This project is carried out under the United States Energy Research and Development Administration Contract No. EY-76-S-02-2421.*000.

3.0 PROGRESS IN INDIVIDUAL TASKS

Progress in each of the three different tasks is reported in the following pages under their individual headings.

During the current reporting period two technical papers were prepared:

1. STRESS CORROSION CRACKING AND ANODIC BEHAVIOR OF AISI 304 STAINLESS STEEL, INCONEL 600, AND INCOLOY 800 STRAINING IN BOILING NaOH SOLUTIONS; Y.S. Park, J. R. Galvele, A. K. Agrawal and R. W. Staehle.
2. INHIBITIVE EFFECT OF SODIUM SALTS ON THE STRESS CORROSION CRACKING OF TYPE 304 STAINLESS STEEL IN BOILING 20 N NaOH SOLUTION Y. S. Park, A. K. Agrawal and R. W. Staehle

preprints removed

The first paper has been submitted to Corrosion Journal for publication, and the second paper will be shortly submitted to Journal of Electrochemical Society. The above two papers are reproduced here under Task 1.

Task 1 - Fundamental Measurements of Stress Corrosion Cracking Parameters Including Inhibitors.

STRESS CORROSION CRACKING AND ANODIC BEHAVIOR OF AISI 304 STAINLESS STEEL, INCONEL 600, AND INCOLOY 800 STRAINING IN BOILING NaOH SOLUTIONS

Y.S. Park, J.R. Galvele*, A.K. Agrawal and R.W. Staehle
The Ohio State University
116 West 19th Avenue
Columbus, Ohio 43210

INTRODUCTION

One generally accepted mechanism of stress corrosion cracking (SCC) states that the essential condition for cracking is film rupture, as a result of slip process, and subsequent anodic dissolution of the exposed bare metal (1). For such a mechanism it should be possible to predict, by constant potential straining experiments, the crack propagation rate (CPR). A quantitative correlation between CPRs calculated from straining experiments, and those from conventional measurements has been reported for: mild steel in boiling nitrate solutions (2); mild steel in boiling NaOH solutions (3); AISI 304 in HCl solutions (4); and for AISI 304 in mixtures of NaCl plus H_2SO_4 solutions (5). It was also shown (4, 5) that the straining experiments could be used to predict morphological features like generalized corrosion, fissuring and sharp cracking.

The aim of the present work was to apply the straining electrode technique to other systems for which SCC has been studied by more conventional techniques. The systems chosen were AISI 304 stainless steel, Incoloy 800 alloy and Inconel 600 alloy, all of them in boiling NaOH solutions. Failure time and crack morphology for these systems was studied with a constant load technique at the Ohio State University (6-10). The results of the present work showed that through short time straining experiments knowledge about CPRs and crack morphology could be gained in good correlation with the results reported from the constant load experiments.

EXPERIMENTAL

Materials and solutions

The samples, heat treatments and solution compositions used were chosen to reproduce the experimental conditions of previous SCC work. The 0.48 diameter wire specimens of AISI 304 stainless steel used were vacuum annealed, in quartz capsules, for 2 h at 1200°C and water quenched. This heat treatment developed a structure with relatively large grains (size ASTM 6). Specimens of Inconel 600 alloy were made from 0.49 mm diameter wire, which were vacuum annealed in quartz capsules for 3 h at 1120°C and water quenched. Incoloy 800 alloy wire specimens 0.38 mm in diameter were annealed in the same way as Inconel 600 alloy.

Test solutions were prepared with reagent grade NaOH and double distilled water. Solutions of 20N NaOH were used in the experiments with AISI 304 stainless steel, and 17.5N NaOH solutions were used with Inconel 600 and Incoloy 800 alloys. No attempt was made to deaerate the solutions, since in the concentrated caustic solutions little dissolved oxygen would be expected under boiling conditions.

Experimental procedure

A Teflon cell, with external heating tape, described in previous publications (7, 9) was used. The annealed specimens were degreased with acetone, rinsed with double distilled water, and mounted in the cell. The solution was heated to about 70°C in a polyethylene container then poured into the cell, where it was heated up to the boiling point. It took about 30 min. for the solution in the cell to reach the boiling point. A platinum counter electrode was immersed in the cell, and the cell was connected to an external Hg/HgO/20N NaOH reference electrode,

through a nylon bridge. All the potentials are reported in the standard hydrogen electrode scale.

The ends of the wire specimens were fixed to an Instron-1130 machine, leaving a gauge length of about 17.0 cm in the cell. A load cell was used to record the load on the specimens during straining. To assure that during the stretching of the wires, no new metal surface entered the cell, the cell was mounted on a pulley system and was hung from the top moving chuck of the Instron machine.

Before starting the straining process, a desired potential was applied to the specimen with a potentiostat, and the current was recorded. Once the current reached a quasistationary value in 5 to 10 min., the straining was started. Cross head speeds of 4, 10, and 20 cm/min were used, giving initial strain rates of about 20, 55, and 110%/min.

CPR Calculation

The calculation of the CPR from the straining experiments was described in a previous publication (4). The current density on the static specimen, i_s, was assumed to be constant during straining on the filmed metal surface. All the current changes observed during straining were attributed to the dissolution of the newly exposed bare metal where the film had broken. The current density measured during straining, i_y, was given by:

$$(i_s \times A_s) + (i_b \times A_b) = i_y \qquad (1)$$

i_s being the current density on the filmed metal, A_s the fraction of specimen area covered by the film, i_b the current density on the bare metal, A_b the fraction of specimen with bare metal, and i_y the current density measured during straining. The i_s and i_y are experimental values.

To calculate i_b, an evaluation of A_s and A_b is necessary. It was found (4) that the bare surface, at a given time, is related to the wire elongation by the following equation:

$$\% \text{ Bare surface} \simeq 1/2\% \text{ Elongation} \qquad (2)$$

Thus, for an elongation of 10%, the bare surface is 5% of the total surface, i.e., $A_s = 0.95$, and $A_b = 0.05$. Equation (2) was developed for an ideal case, where a ductile metal covered by an adherent but brittle film was strained (11). Deviations from this ideal should be expected because of changes in the slip morphology, film ductility and lack of adherence, etc. However, in SCC work the CPR and the failure time are always reported in logarithmic scales, and often data are widely scattered. Therefore, for the technique described in the present paper, the above approximations are considered reasonable. Nonetheless, in those cases where data was available (2, 3, 5) very good agreement was found between the CPRs measured conventionally and those calculated from the straining experiments.

The CPR (m/s) was calculated from the i_b value by the following equation:

$$CPR = \frac{i_b \cdot E \cdot 10^{-2}}{F \cdot d} \qquad (3)$$

where E is the mean equivalent weight of the alloy, F the Faraday constant, and d the density of the alloy. For AISI 304 stainless steel, assuming the formation of Fe^{+2}, Cr^{+3} and Ni^{+2}; E = 25.2; thus for a current density $i_b = 10^{-1}$ A/cm^2 the calculated CPR is 3.3×10^{-8} m/s. At high electrode potentials, if the dissolution products are Fe^{+3}, Cr^{+6}, and Ni^{+2}, the mean equivalent weight for AISI 304 would be 15.9. The mean equivalent weight used for Incoloy 800 alloy was E= 25.1, and Inconel 600 alloy E = 26.5.

RESULTS

AISI 304 Stainless steel in 20N NaOH solution

Anodic current transients were observed during the straining of AISI 304 at constant potential in boiling 20N NaOH solution. Figure 1 shows typical results of the straining experiments. Three types of transients were observed: in the active region, -0.80 V_H, the initial current density was high, and the straining of the wire only caused a small increase in i_y; in the passive region, -0.52 V_H, straining had a large effect on the current density i_y, but the currents involved were small; on the other hand in the transpassive region, 0.00 V_H, the initial current was high, and straining of the wire produced much higher currents.

From the changes in the current density during straining, the current density on the bare metal, i_b, was calculated. Figure 2 shows the initial current density, i_s, and the current density on the bare metal, i_b, calculated at 10% elongation for three different strain rates. The polarization curve of AISI 304 in NaOH solution, as given by i_s, shows an active region from the corrosion potential up to about -0.8 V_H, a passive region between -0.8 and -0.3 V_H, a transpassive region from -0.3 to -0.1 V_H and a secondary passive region above -0.1 V_H. As shown in Figure 2, i_b is affected by the strain rate, but in all the cases values are of the same order of magnitude. In the active region and in the secondary passive region, i_b values for the two highest strain rates are almost identical. On the other hand, in the passive region i_b is strongly dependent on the strain rate, indicating that the repassivation rate of the bare metal in this zone is higher than that in the active and secondary passive regions. At about -0.15 V_H i_s and i_b are equal; i.e., the straining of the metal had practically no effect on the current density.

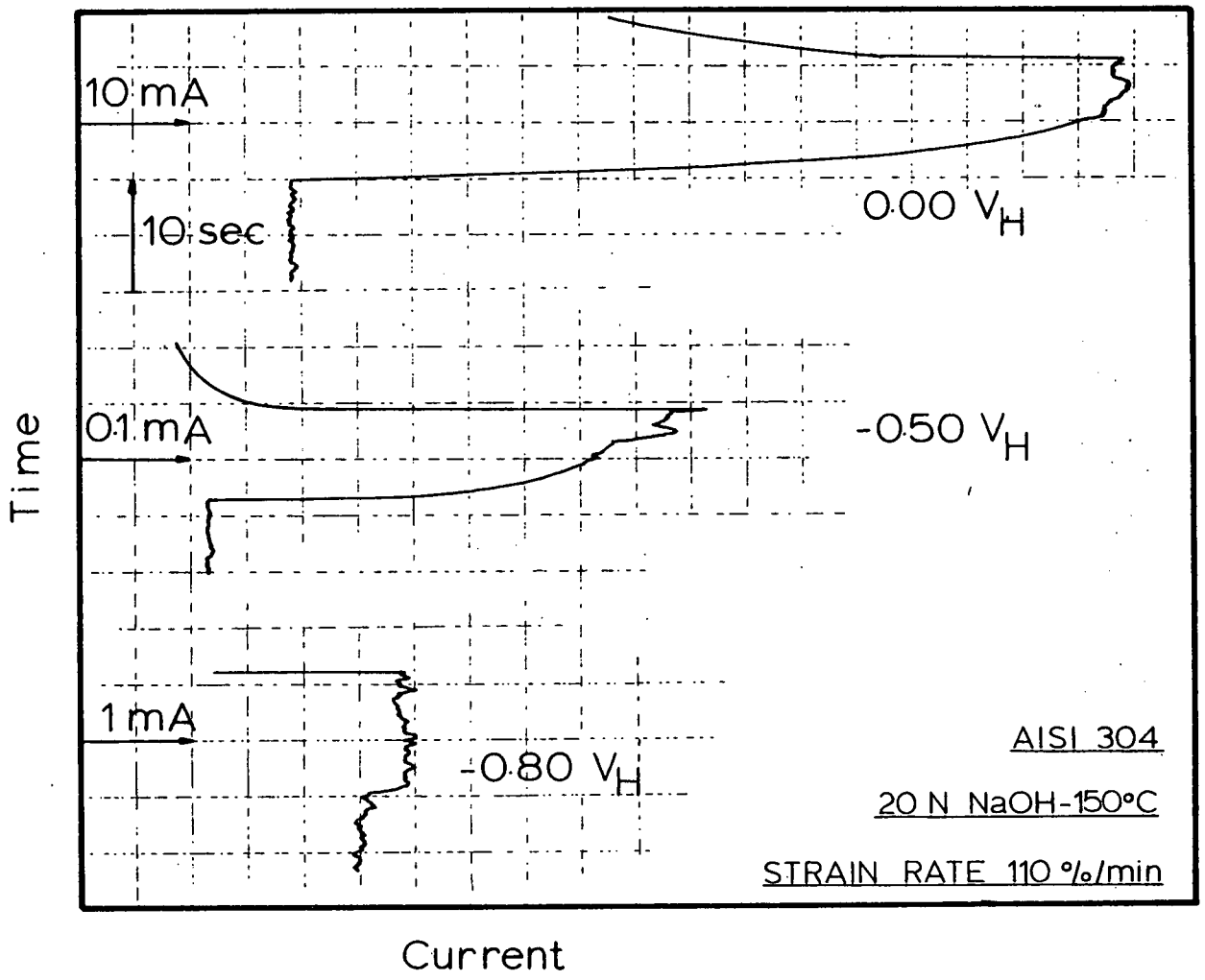

Figure 1 Typical current-time curves for AISI 304 stainless steel strained in boiling 20N NaOH solution. Initial strain rate 110%/min.

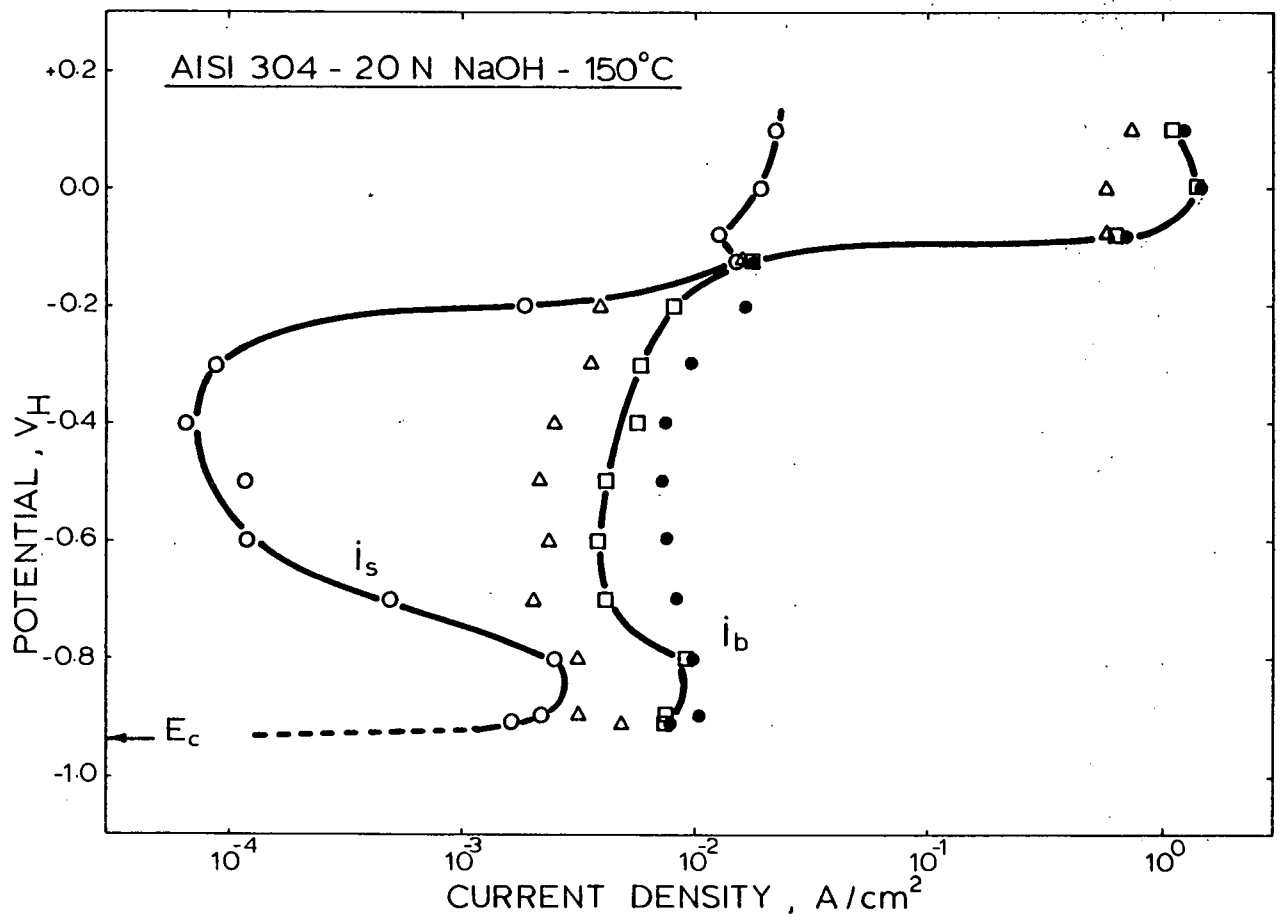

Figure 2 The current density on the filmed metal, i_s, and the calculated current density on the bare metal, i_b, at different potentials for AISI 304 stainless steel strained in boiling 20N NaOH solution. Strain rates used: Δ, 20%/min; □, 55%/min; and ●, 110%/min. E_c: corrosion potential.

The SCC behavior of AISI 304 in boiling 20N NaOH solution has been studied using a constant load technique by Subrahmanayam et al (6) and by Park, Agrawal and Staehle (7, 8). Figure 3 shows a compilation of their results. It is evident that the failure time is strongly affected by the potential. The failure time was short near the corrosion potential, with an increase in potential the failure time improved up to the passive region, where no failures occurred. Near the transpassive region the failure time started to decrease, and in the secondary passive region eventually dropped to values lower than those found at the corrosion potential. The morphology of the attack, also shown in Figure 3, near the corrosion potential resembled dense fissuring, leading to almost generalized corrosion. In the passive region the non-failed specimens showed incipient cracking. At these potentials the cracks were more localized than in the active region, but the propagation rate was very small. In the transpassive region the specimens did not fail by cracking but by extensive pitting which led to uniform thinning. No cracks were detected in this region. In the secondary passive region deep cracks were found along with considerably short failure times.

No direct CPR data are available for this system; but the failure time data in Figure 3 can be used for an evaluation of the potential dependence of the CPR. Figure 4 shows the CPR values calculated from i_b, using the 55%/min strain rate results. The calculated CPR for the passive region is very small, $\sim 2 \times 10^{-9}$ m/sec, which is in accord with the non-failures reported by Park, Agrawal and Staehle. Below the passive zone, $< -0.7\ V_H$, a reduction in the failure time is observed. The straining experiments show a concordant increase in the CPR for this region. In the secondary passive region extremely short failure times are again in complete accord with the high CPRs found by the straining experiments.

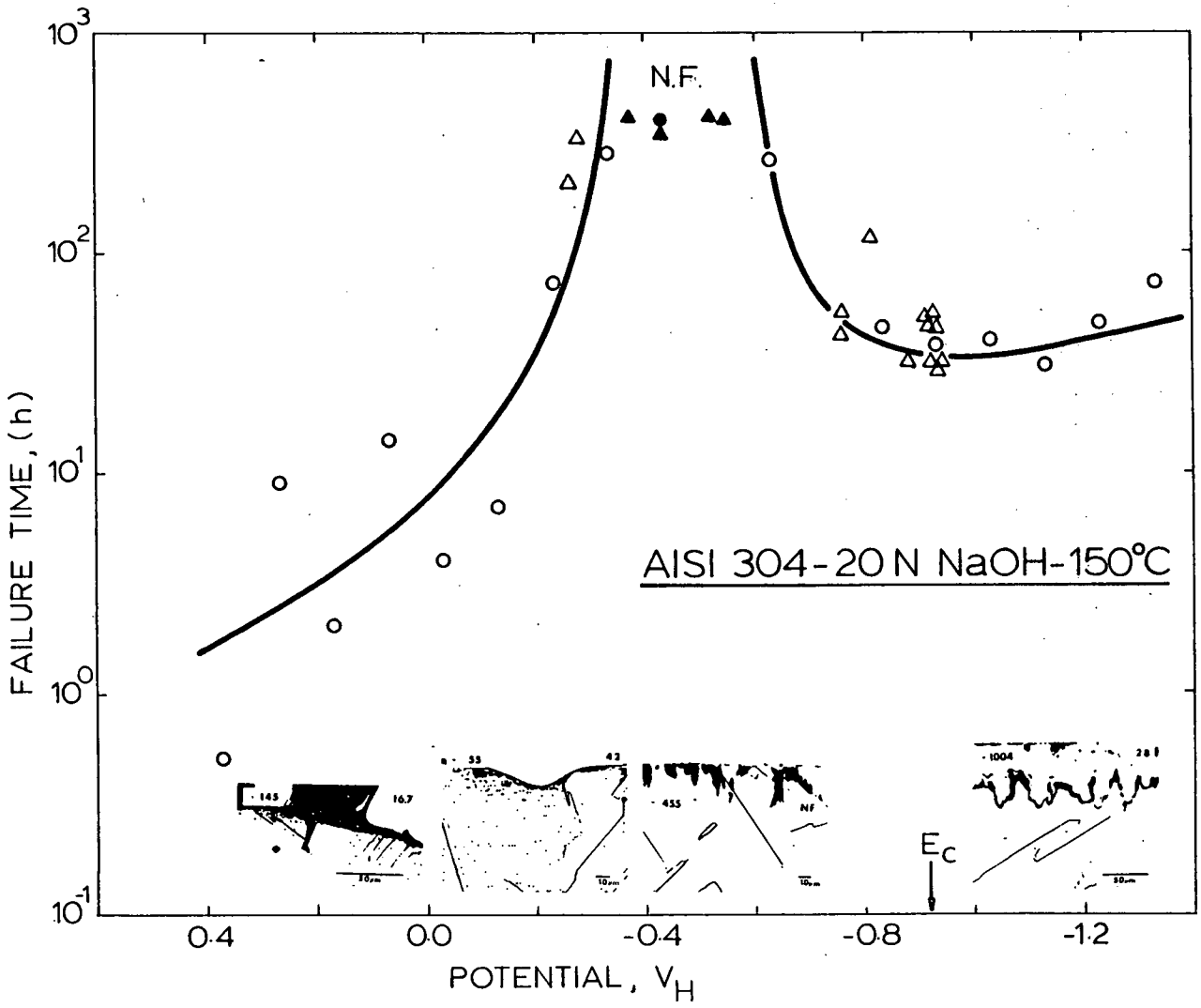

Figure 3 The failure time and crack morphology at different potentials for AISI 304 stainless steel in boiling 20N NaOH solutions; ●, 20N NaOH; ∆, 20N NaOH + 0.005M $CrO_4^=$. After Park et al (7, 8).

In recent publications (4, 5) it was shown that the i_b/i_s ratio could be used to evaluate the corrosion morphology. A high current ratio would indicate that the corrosion on the bare metal is much higher than that on the filmed metal. This would mean sharp cracking. On the other hand, a low current ratio indicated that the corrosion rate on the bare metal is similar to that on the filmed metal. Under this condition, fissures, with a tendency to generalized corrosion, should be expected. Finally, if the ratio was equal to one, no localized corrosion should be found.

Figure 4 shows also the i_b/i_s values calculated for AISI 304 from the data in Figure 2. In the passive region the ratio is high, indicating that sharp cracks should be expected. But, since the CPRs are very small, only incipient cracks should be found, such as those reported by Park, Agrawal and Staehle. Near the corrosion potential the CPR increased slightly but the i_b/i_s ratio decreased; this suggests fissuring with a tendency to generalized corrosion, again in agreement with the results of Park et al.

In the secondary passive region rapid SCC should be expected, because both the current ratio i_b/i_s and the CPR are high. But in the transpassive region while the CPR increased, the current ratio dropped to one. This indicates that a decrease in the failure time should be expected, but no cracks should be found, as actually reported by Park et al.

Incoloy 800 alloy in 17.5N NaOH solution

Figure 5 shows i_s and i_b values for Incoloy 800 alloy straining in boiling 17.5N NaOH solution. Active, passive, transpassive and secondary passive regions were found for the alloy, in agreement with the previous work (9, 10). The i_b value was affected by the strain rate in a way similar to that for AISI 304 in 20N NaOH, the effect being more noticeable

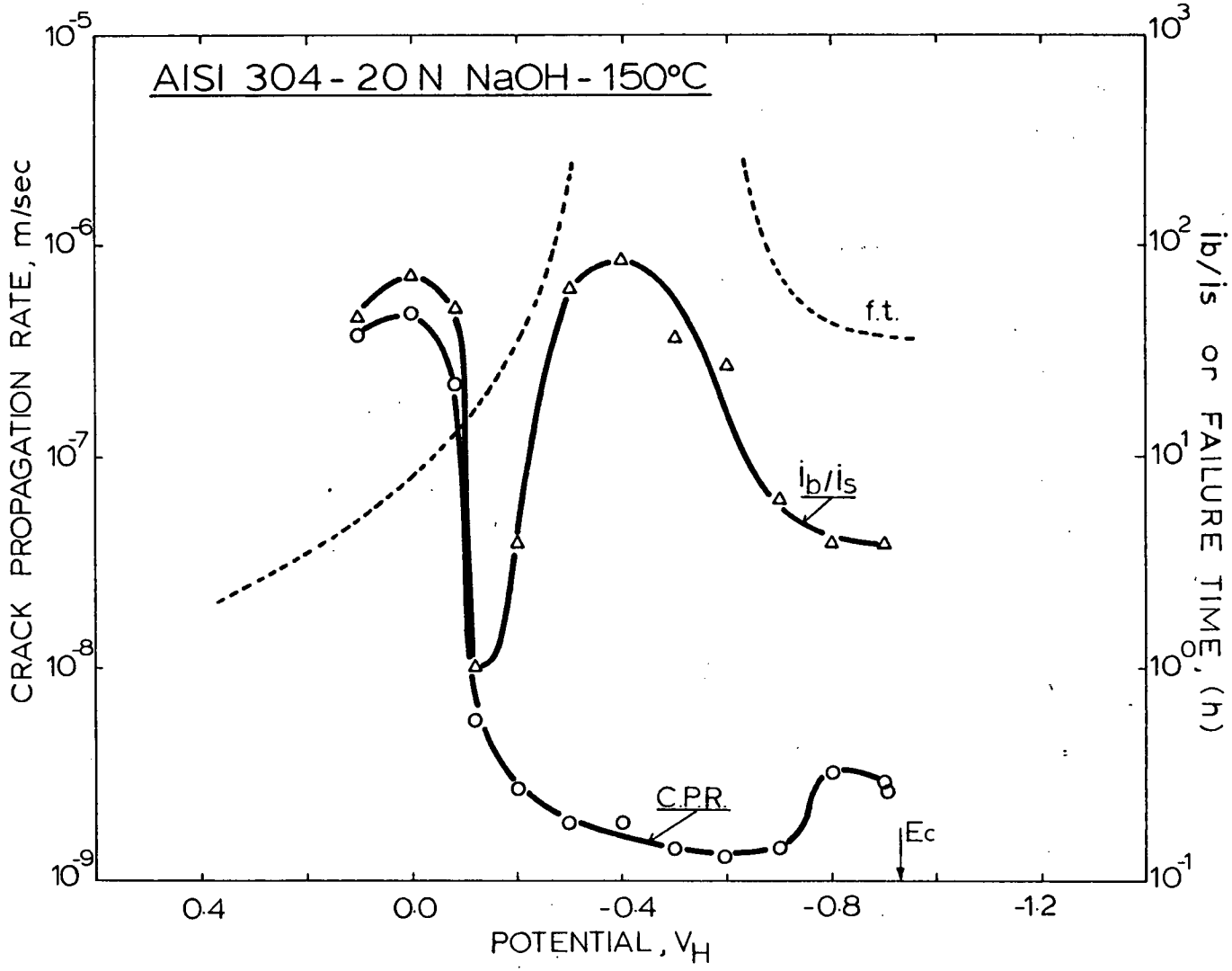

Figure 4 Calculated crack propagation rate and current ratio i_b/i_s at different potentials for AISI 304 stainless steel strained in boiling 20N NaOH solution. Dotted line: failure time values from Figure 3.

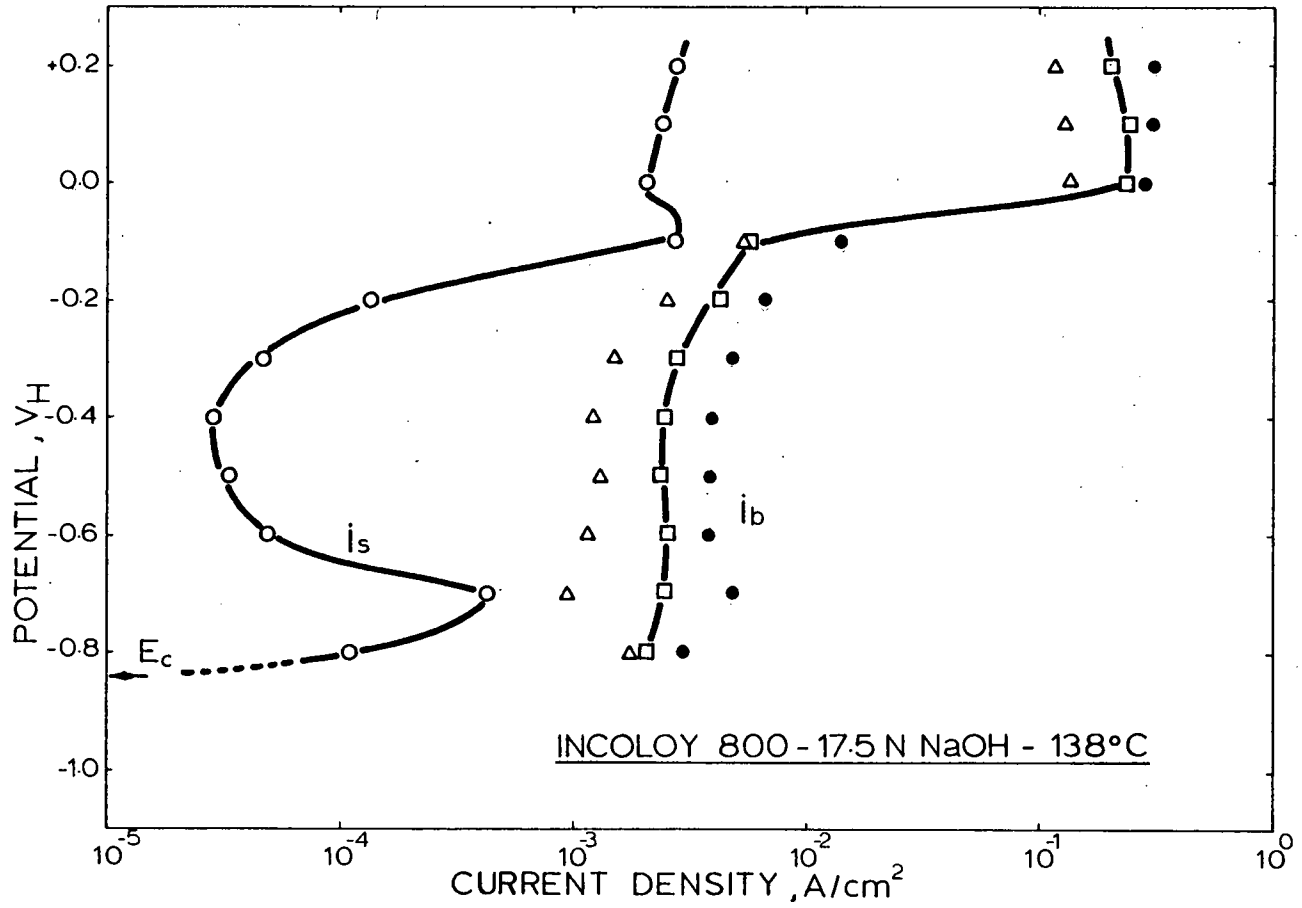

Figure 5 The current density on the filmed metal, i_s, and the calculated current density on the bare metal, i_b, at different potentials for Incoloy 800 alloy strained in boiling 17.5N NaOH solution. Strain rates used: Δ, 20%/min; □, 55%/min; and ●, 110%/min. E_c: corrosion potential.

in the passive region. Near the corrosion potential, as well as in the secondary passive region, the i_b tended to be relatively less affected by the strain rate, especially with the higher strain rates.

The SCC behavior of this system was studied by Liening et al using a constant load technique (9, 10). Their failure time data at different potentials are shown in Figure 6, against the corresponding CPR and i_b/i_s ratio calculated with the i_b and i_s values from Figure 5. The CPR was lowest at the corrosion potential and increased slightly with an increase in the potential, but in the secondary passive region the CPR jumped suddenly by approximatley two orders of magnitude. The CPR thus inversely follows the failure time trend reasonably well for all potentials above the active peak, i.e., $E > -0.6\ V_H$. However, at the corrosion potential and in the active region the low CPRs indicate high failure times, contrary to the relatively low failure times reported for this region.

The crack sharpness ratio i_b/i_s for this system was lowest in te transpassive region, $\sim -0.10\ V_H$, suggesting a nonlocalized or uniform corrosion for this region, which is in conformity with the morphology observed by Liening et al. The next lowest value was in the active region, supporting again the reported general corrosion for this region. An intermediate value of i_b/i_s near the corrosion potential suggests fissuring or localized attack, which also reasonably matched with the morphology observed from the constant load experiments. The i_b/i_s ratio was considerably high, $\sim$100, in both the passive and the secondary passive regions and indeed very sharp cracks were observed in these regions by Liening et al.

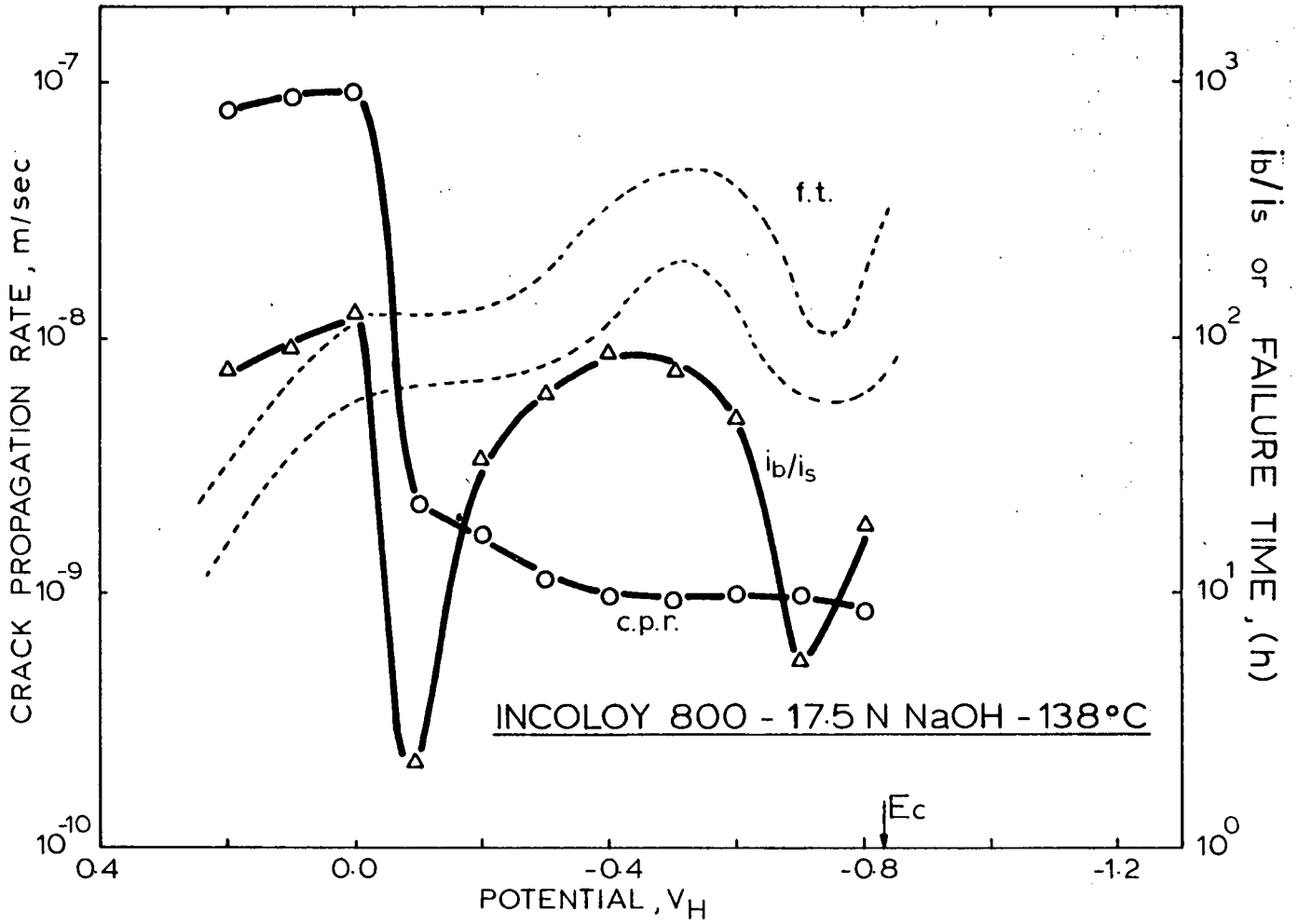

Figure 6 Calculated crack propagation rate and current ratio i_b/i_s at different potentials for Incoloy 800 alloy strained in boiling 17.5N NaOH solution. E_c: corrosion potential. Dotted line: failure time values after Liening et al (9, 10).

Inconel 600 alloy in 17.5N NaOH solution

Figure 7 shows the results from the straining experiments for Inconel 600 alloy in boiling 17.5N NaOH. The general features are similar to those found for Incoloy 800 in the same solution. The main difference is that near the corrosion potential the i_b value for Inconel 600 is an order of magnitude higher than the corresponding value for Incoloy 800.

The calculated CPR and i_b/i_s values at different potentials are shown in Figure 8, in relation to the failure times reported by Liening et al for the same system. No failures were observed by Liening et al in the passive potential region, -0.3 to -0.5 V_H; the calculated CPR values for this region are indeed low, $<10^{-9}$ m/s, and therefore in support of the failure time data. Near the corrosion potential the failure time was low; this is correctly reflected in the calculated CPR, which is an order of magnitude higher than that in the passive region. Above the passive region and up to ~0.0 V_H Liening et al have reported a decreasing trend in the failure time with potential; the calculated CPR shows an increase with potential which correlates reasonably with the failure time trend. Only above ~0.0 V_H the high CPR values are not in conformity with the high failure times.

The i_b/i_s values in Figure 8 are uniformly high, ~60, over the entire potential range studied, particularly in the transpassive region where values are above 100. The high i_b/i_s values for Inconel 600 suggest intense localized attack over most of the potential occured. Liening et al have reported pitting and grain boundary grooving as the principal mode of attack on Inconel 600 in boiling 17.5N NaOH. Only in the transpassive region, >-0.25V_H, where the i_b/i_s value is least, ~35, a nonlocalized attack, i.e., uniform corrosion was observed.

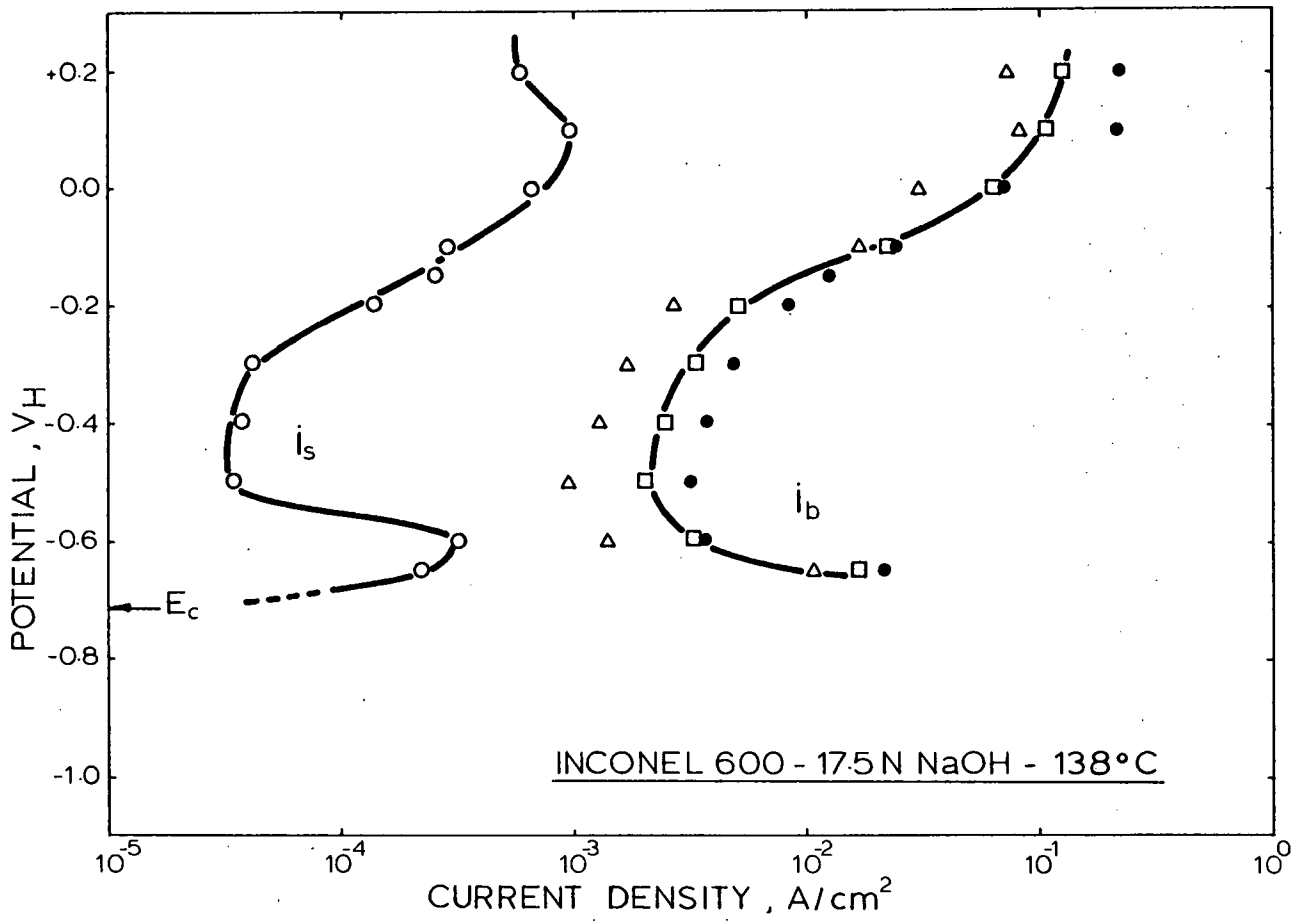

Figure 7 The current density on the filmed metal, i_s, and the calculated current density on the bare metal, i_b, at different potentials for Inconel 600 alloy strained in boiling 17.5N NaOH solution. Strain rates used: Δ, 20%/min; □, 55%/min; and , 110%/min. E_c: corrosion potential.

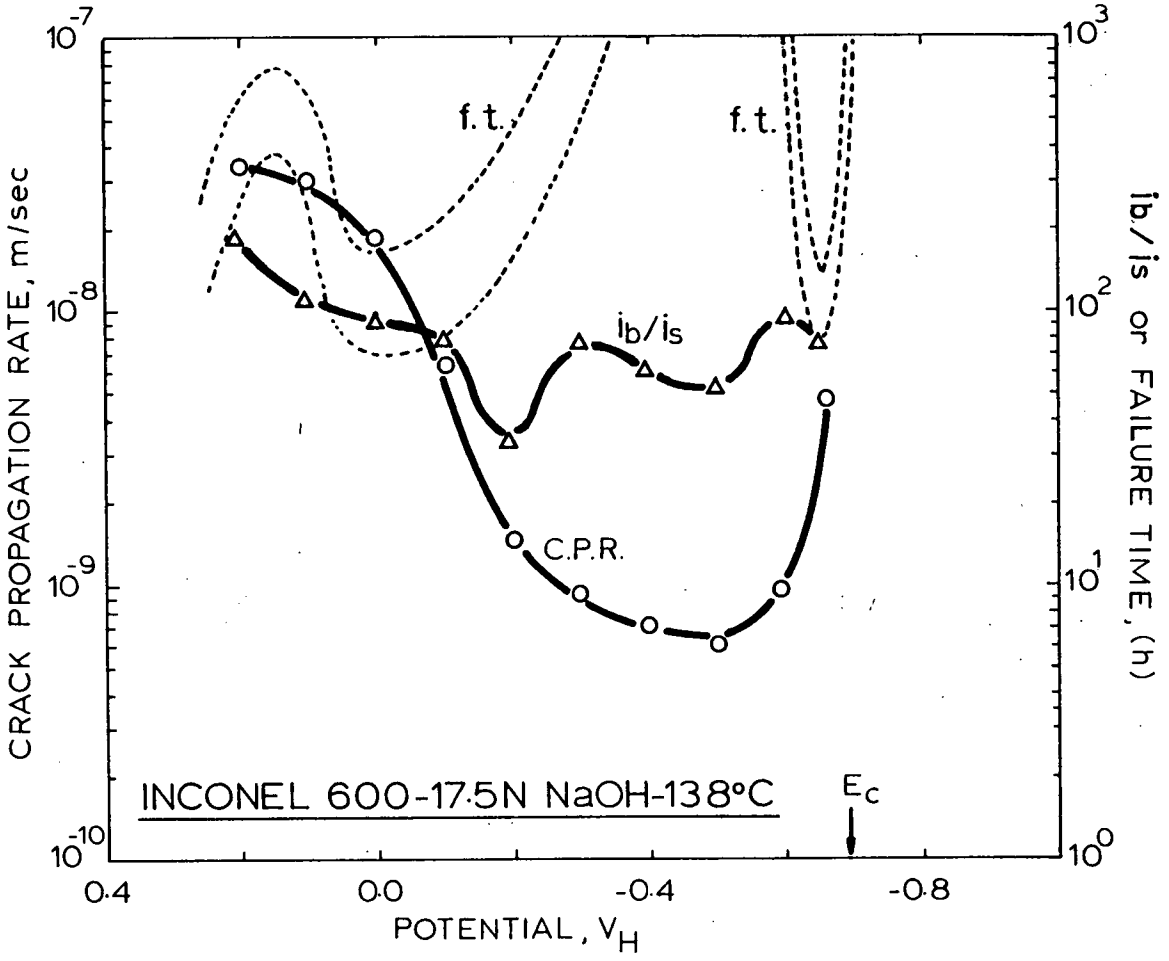

Figure 8 Calculated crack propagation rate and current ratio i_b/i_s at different potentials for Inconel 600 alloy strained in boiling 17.5N NaOH solution. E_c: corrosion potential. Dotted line: failure time values after Liening et al (9, 10).

DISCUSSION

A reasonably good correlation between the failure times observed from the constant load experiments and the CPRs calculated from the straining experiments at different potentials for the alloys AISI 304, Incoloy 800 and Inconel 600 attests to the usefulness of the straining technique. A one to one correspondence between the failure time and the CPR should not be expected over the entire potential range for the alloys; principally, because the observed failure time includes both the crack initiation time and the cracking time, and the former may also vary with the potential. This may be one reason for the anomoly observed for Inconel 600 alloy in the secondary passive region, E>0.0 V_H, where the high CPRs are not reflected in the short failure times in the constant load experiments. The CPRs for Incoloy 800 alloy are practically the same from the corrosion potential up to the beginning of the secondary passive region. However, the failure time near the corrosion potential are considerably shorter than in the passive region. Here, a drop in the initiation time near the corrosion potential could have yielded shorter failure times as compared with those in the passive region.

The repassivation rate can be estimated from the effect of strain rate on i_b; a strong dependence of i_b on the strain rate, similar to that observed for all three alloys in the passive region, suggests fast repassivation. On the other hand little or no change in i_b with the strain rate, similar to that for AISI 304 steel (for 55 and 110%/min) in the active and in the secondary passive regions, suggests either an absence of or a slow repassivation process. If the initiation time be considered related to the repassivation rate of the metal, a fast repassivation rate would lead to a long initiation time, and a slow repassivation rate to a short initiation time. In the case of Inconel 600 alloy the i_b values in the secondary passive region are

strongly dependent, unlike that for Incoloy 800 alloy and AISI 304 steel in the same potential region, upon the strain rate (compare Figures 2, 5 and 7). Thus, long failure times observed for Inconel 600 alloy in the secondary passive region, in spite of high calculated CPRs, are due to the fast repassivation rate or long initiation time. On the other hand, the small effect of the strain rate on the i_b of Incoloy 800 near the corrosion potential indicated a lack of repassivation or short initiation time. This supports a shorter failure time than in the passive region for the same CPRs.

The CPRs and i_b/i_s ratios of AISI 304 steel, Inconel 600 alloy and Incoloy 800 alloy are shown together as a function of potential in Figure 9 for comparison purposes. It should be noted that the AISI 304 steel was studied in 20N NaOH at 150°C whereas the other two alloys were investigated in 17.5N NaOH at 138°C. However, the effect of a slight increase in concentration and temperature of nearly saturated caustic solution, such as 17.5N NaOH, on the current densities of the alloys may be only incremental, and therefore may be ignored for qualitative comparison. It is clearly seen in Figure 9 that the CPR plots of all the three Fe-Cr-Ni alloys follow an almost identical pattern. In general, the CPRs for any alloy are lowest ca. 10^{-9} m/s in the passive region, intermediate ca. 3×10^{-9} m/s in the active region and highest ca. $>10^{-8}$ m/s in the secondary passive region.

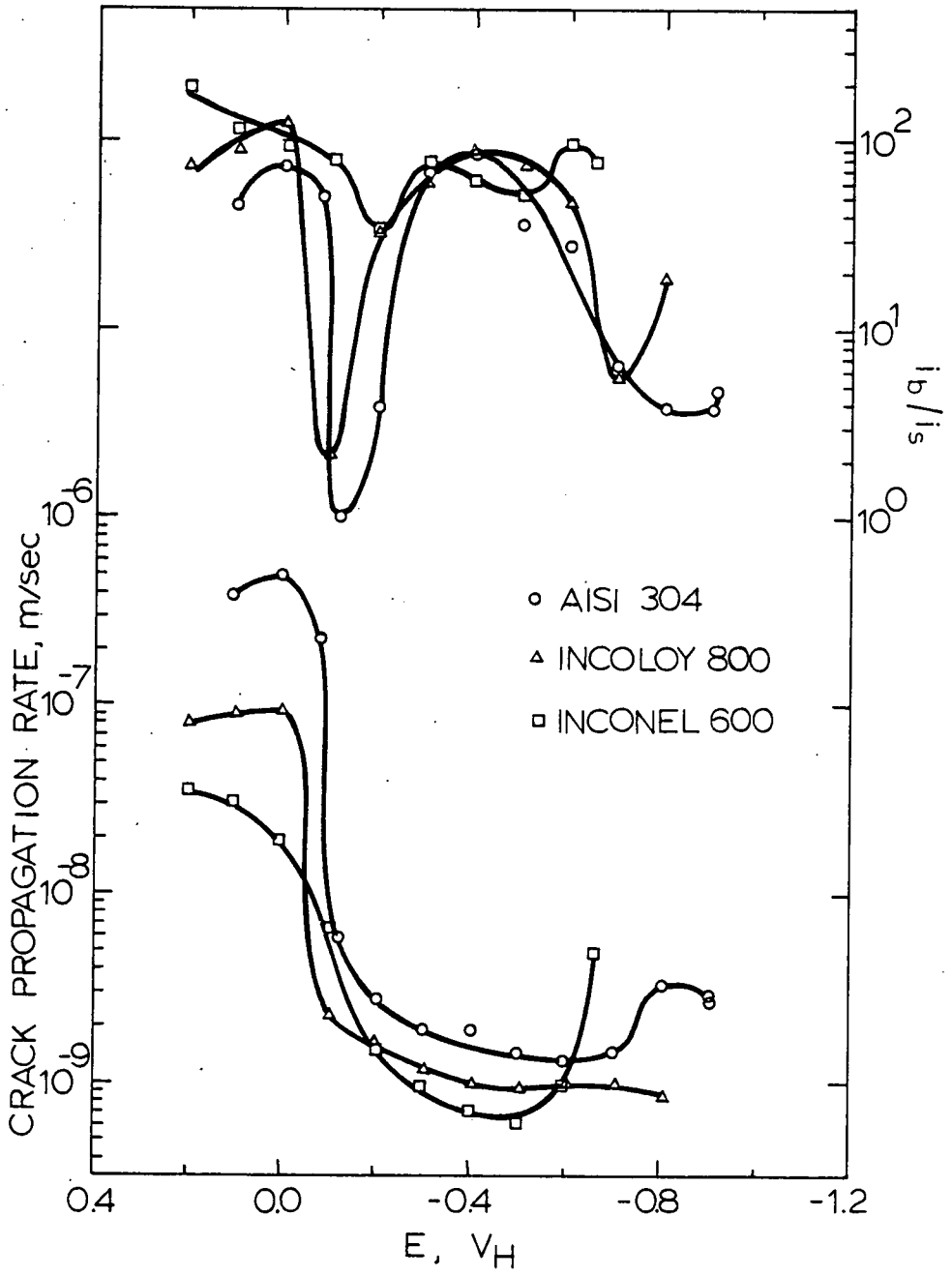

Figure 9 The CPR and i_b/i_s ratio as a function of potential for the alloys AISI 304 in 20N NaOH and Inconel 600 and Incoloy 800 in 17.5N NaOH solution.

The relative CPRs of the alloys at any potential appear to be directly related to the composition of the alloy. The relationship is qualitatively shown below:

Potential Region	CPR Trend	Controlling Element
Active	I-600 > AISI 304 > I-800	
	15 < 18 < 20	Cr%
Passive	AISI 304 > In-800 > In-600	
	10 < 30 < 75	
Transpassive	In-600 > AISI 304 > In-800	
	15 < 18 < 20	Cr%
Secondary Passive	AISI 304 > In-800 > In-600	
	10 < 30 < 75	Ni%

The CPR in the active region follows the decreasing Cr content, i.e., the highest rate is for the alloy Inconel 600 having the lowest Cr, and the lowest rate is for the alloy Incoloy 800 with the highest Cr content. The CPRs in the passive and the secondary passive regions decreased with an increase in the nickel content, the effect being especially noticeable in the latter region, Figure 9. The element controlling the CPR in the transpassive region is not so discernable; it could be either Cr or Ni. The constituent element which has the lowest dissolution rate at the potential of interest appears to control the CPR of the alloy. This will be evident on examining Figure 10, where the polarization curves of pure elements Fe, Cr and Ni in 17.5N NaOH at 130°C are shown. The current density for Cr in the lower potential region of the polarization curves is about one order of magnitude less than for Ni and two orders of magnitude less than for Fe. In the upper potential region the current density for Ni is about one order of magnitude less than for Fe, and two orders of magnitude less than for Cr. These observations clearly support the effect of alloying elements on the CPR.

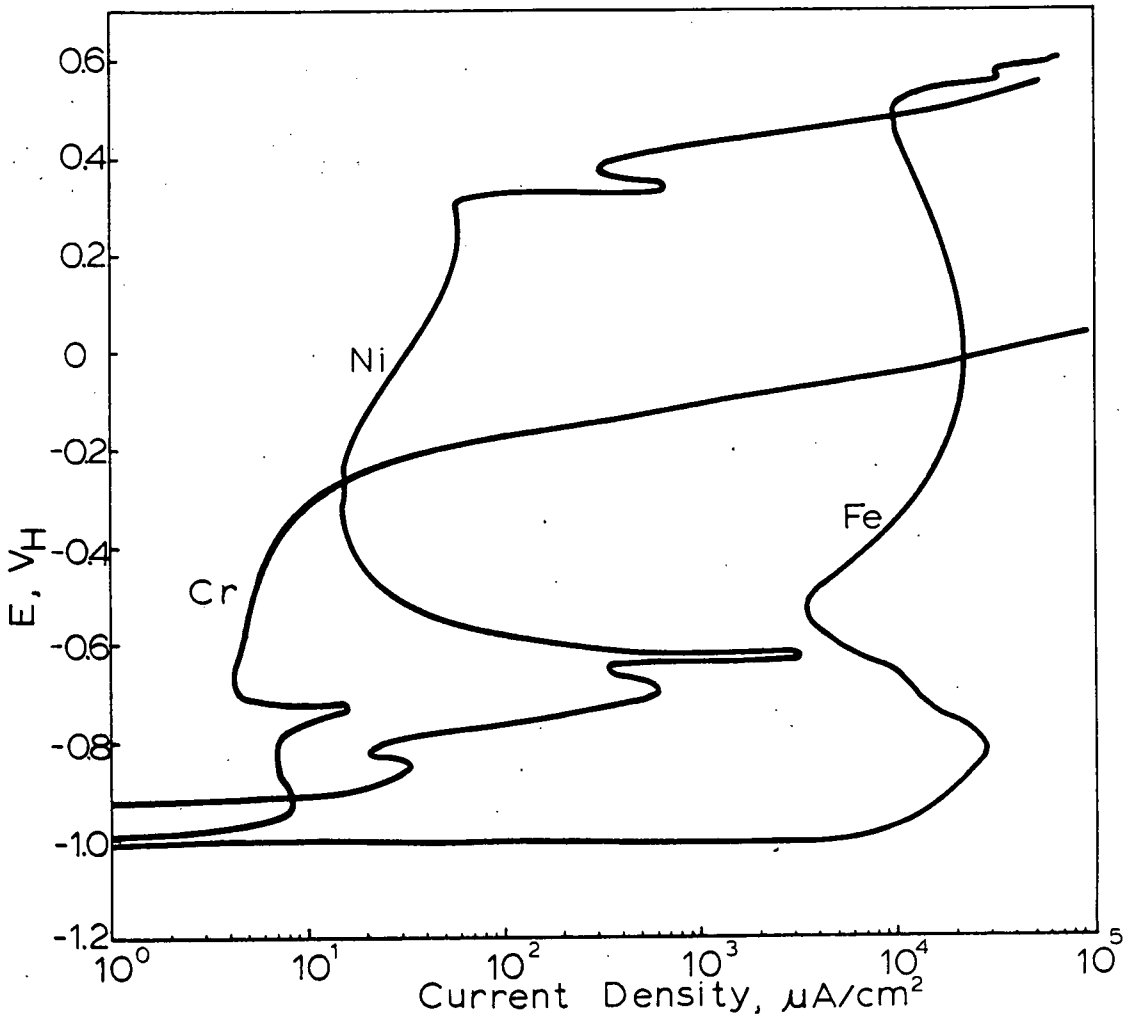

Figure 10 The polarization behavior of pure elements Fe, Cr and Ni in 17.5N NaOH at 130°C (15).

The i_b/i_s ratio vs. potential plots for the three alloys in Figure 9 also show a somewhat regular pattern. The ratio is highest, ca. 50, for the alloys in their respective passive and the secondary passive regions, and lowest in the transpassive region. The high ratios indicate intense localized attack as actually seen for all the three alloys at their corresponding potentials. The lowest ratio in the transpassive region in all cases matched the observed uniform corrosion. The ratios in the active region of alloys AISI 304 and Incoloy 800 fall in an intermediate range between the high and low values, except that for the Inconel 600 alloy which is in the high range. In the active region, for the intermediate i_b/i_s ratios fissuring was observed, but with high ratio for Inconel 600 alloy the attack was intensely localized as expected.

The values of the i_b/i_s ratio were grouped above into "high" or "low" based on the relative height of the ratio in the i_b/i_s vs. potential plot for the alloy environment system under consideration. Since the quality of film, e.g., ductility, porosity and adherence, etc., may vary from one system to another, it is not possible to assign absolute numbers for characterizing the i_b/i_s ratios. In the present case, for example, in the transpassive potential region where all the three alloys failed under constant load by general corrosion, the lowest i_b/i_s ratio increased with an increase in the nickel content of the alloy, i.e., the ratio was one for AISI 304 steel, two for Incoloy 800 alloy and 34 for Inconel 600 alloy. Furthermore, i_b and therefore the i_b/i_s ratio is strain rate dependent; implications of which are discussed in the following paragraphs. The usefulness of i_b/i_s analysis lies in the fact that it provides a quick means for evaluating the intensity of localized attack at different potentials with respect to a known standard. However, conventional SCC experiments and fractography are recommended for critical answers as to whether the specimen will fail intergranularly or transgranularly.

The current density on the bare metal, i_b, as mentioned above, depends to a good extent on the strain rate, especially in the passive region. Murata and Staehle (12) and also Wexler and Galvele (13) have reported that the current density on a straining metal in the passive region shows a linear dependence on the strain rate. This puts a limitation on the strain rates that can be used for SCC evaluation, because a very high strain rate would lead to misleading CPRs. On the other hand, Hoar and Jones (3) have reported that at very slow strain rate the repassivation of the bare metal will be significant, thus giving very low CPRs even in the regions of high SCC susceptibility. Hoar and Jones found that, for mild steel in caustic solutions, the strain rate should be approximately 100%/min. At this strain rate the repassivation of the bare metal is minimum, and the calculated CPR correlates very well with other SCC evaluation techniques.

An optimum strain rate for the Fe-Cr-Ni alloys in the present case also appears to be between 55 and 110%/min. The i_b values in the active region are practically in the limiting range with the above strain rates. The CPRs calculated with the 55%/min strain rate data are of the order of 10^{-10} - 10^{-9} m/s below the transpassive region. A CPR of 10^{-10} - 10^{-9} m/s is taken as the minimum rate in other SCC evaluation techniques, for example in the definition of K_{ISCC} with precracked specimens (14). Thus higher strain rates would give misleading high CPRs in the passive region, by over-compensating the repassivation kinetics.

CONCLUSIONS

The following conclusions may be drawn from the present investigation.

1. The straining electrode technique is a useful method for a rapid determination of CPR and an estimation of crack morphology.
2. The CPR of Fe-Cr-Ni alloys in boiling concentrated caustic solutions varies with potential. The maximum rate for an alloy was calculated in the secondary passive region and the minimum in the passive region. The CPR in the active region is higher than in the passive region, but more than one order of magnitude less than in the secondary passive region.
3. An intensely localized attack is predicted for the alloys in their passive and secondary passive regions, but a generalized attack in the transpassive region. Fissuring is expected in the active region with a tendency for greater localization with increasing nickel content in Fe-Cr-Ni alloys.
4. The CPR of an Fe-Cr-Ni alloy in caustic solution appears to be controlled by the alloying element which has the lowest corrosion kinetics at the potential of interest. The percentage of element required in an alloy to control its kinetics was not determined in this study; the straining electrode technique would be useful for such a determination.
5. The CPR of the three Fe-Cr-Ni alloys in caustic solution near their respective corrosion potentials may be arranged in the following order of increasing Cr content: Inconel 600 > AISI 304 > Incoloy 800. But due to longer crack initiation time in Inconel 600, it may be more resistant to SCC than AISI 304.

REFERENCES

1) R. W. Staehle, in "Stress Corrosion Cracking and Hydrogen Embrittlement of Iron Base Alloys", Editors: R. W. Staehle, J. Hochmann, R. D. McCright, and J. A. Slater, NACE (1977).

2) T. P. Hoar and J. R. Galvele, Corrosion Sci. 10, 211 (1970)

3) T. P. Hoar and R. W. Jones, Corrosion Sci. 13, 725 (1973)

4) J. R. Galvele, S. B. de Wexler and I. Gardiazabal, Corrosion, 31, 352 (1975).

5) J. R. Galvele and I. Maier, in "Passivity and Its Breakdown on Iron and Iron Base Alloys," p.178, Editors: R. W. Staehle and H. Okada, NACE (1976).

6) D. V. Subrahmanayam, A. K. Agrawal and R. W. Staehle. To be published. See also R. W. Staehle, in "The Theory of Stress Corrosion Cracking of Alloys," p.228, Editor: J. C. Scully, NATO (1971).

7) Y. S. Park, M.S. Thesis, Ohio State University (1975).

8) Y. S. Park, A. K. Agrawal and R. W. Staehle, 149th Meeting Extended Abstracts, p. 109, The Electrochemical Society (1976).

9) E. L. Liening, M.S. Thesis, Ohio State University (1974).

10) E. L. Liening, A. K. Agrawal and R. W. Staehle, to be published.

11) S. F. Bubar and D. A. Vermilyea, J. Electrochem. Soc., 113, 892 (1966)

12) T. Murata and R. W. Staehle, in "5th International Congress on Metallic Corrosion", Japan, NACE (1974).

13) S. B. Wexler and J. R. Galvele, J. Electrochem. Soc., 121, 1271 (1974).

14) M. O. Speidel, in"The Theory of Stress Corrosion Cracking in Alloys" p.301, Editor: J. C. Scully, NATO (1971)

15) U. Kim, unpublished work, Ohio State University (1977).

Task 2 Electrochemical and Corrosion Studies in Aqueous Solutions Containing Sulfide Ions. S. Bradford*, A. K. Agrawal and R. W. Staehle

Introduction

The purpose of this task is to determine the corrosion kinetics of pure metals Fe, Cr, Ni, etc. in aqueous environment containing sulfide ions, in the temperature range 0 - 100°C. The influence of sulfide ion on the active and passive behavior of metals and the nature of surface films is of interest.

In the current reporting period work has been started with pure iron. In order to determine the effect of $S^=$ ion concentration on the corrosion properties of iron Na_2SO_4 solution was selected as the base electrolyte for the polarization studies. The advantage of Na_2SO_4 solution as the base electrolyte is that the $SO_4^=$ ion is stable, kinetically and also thermodynamically, over the entire pH range between 0 and 14. The $SO_4^=$ ion is not easily reduced or oxidized in the potential range of interest, i.e., between the HER and the OER. Further, in sulfide solution some $SO_4^=$ ions are always present as an oxidation product of $S^=$. The pH of Na_2SO_4 solution is easily adjustable between 0 and 14 with either H_2SO_4 or NaOH, for covering a wide pH range for corrosion studies without introducing a foreign ion.

Potentiodynamic polarization curves of pure iron have been established in sulfate solutions at pH values of 0.5 to 13, temperatures of 25 to 85°C, and sulfide ion concentrations of 0 to 300 ppm. Experimental technique and some of the results are described below. Controlled potential coulometric experiments to determine the long range effect of $S^=$ ion on the passive behavior of iron has been started but no significant results are available at the time of reporting. The surface film formed on iron during controlled potential tests in $S^=$ containing solutions will also be analyzed by Auger Spectrometer.

---

*Prof. S. Bradford is at the OSU on a Sabbatical leave from University of Alberta, Canada

Experimental

Iron stock was obtained in the form of 6.25 mm dia. rod of 99.97% purity. Specimens were cut to 10 mm size, these were press fitted in Teflon holders, thus only one face of the rod, area 0.31 cm^2, was exposed. After mounting a specimen it was polished with different grades of SiC papers, ending with a 600 grit paper and a mirror finish. The polished specimen was cleaned with acetone and double distilled water prior to putting in the cell.

An H-type glass cell was used for the polarization studies. The working electrode compartment was separated from the counter electrode compartment by a fine pore glass frit in order to avoid contamination of the test solution with the reaction products generated in the counter electrode compartment during the test. The reference electrode used was Hg/Hg_2SO_4/satd. K_2SO_4 electrode, and the counter electrode was Pt sheet. In order to avoid damage to the reference electrode from sulfide ions, it was placed outside the cell in a compartment which was connected to the cell through a wetted ground glass stopcock and a Luggin capillary. Only the working electrode compartment of the H Cell was heated with heating tapes, and the temperature was controlled to within ± 0.1°C of the set point

Principal instruments used in this study were Wenking potentiostat model 68TS3, Halstrup motorpotentiometer model MP165, and an Esterline Angus strip chart recorder model Eiiois.

Test solutions were made from reagent grade chemicals Na_2SO_4, H_2SO_4, NaOH and Na_2S using double distilled water. The electrolyte for the pH 0.5 runs was 1M H_2SO_4; for the higher pH runs it was 1M Na_2SO_4 with pH adjusted by H_2SO_4 or NaOH additions. Sulfide additions were made by introducing the

proper amount of Na_2S solution into the electrolyte after it had been purged with purified Ar. Purging of the electrolyte was stopped after the introduction of Na_2S. The test solution was introduced into the two cell compartments which had been also purged with Ar.

The specimen was allowed to stand in the test solution for 30 minutes while monitoring its open circuit potential. A potential 500 mV below the rest potential was applied to the specimen and an anodic scan, 25 mV/min., was started. The scan was terminated in the transpassive region of the metal or earlier if the current became too high.

Results

Some typical polarization curves of Fe which demonstrate the effects of pH temperature and sulfide ion concentration on the active-passive behavior of the metal are shown in Figures 1 to 4.

Figure 1 shows the anodic polarization curves at 25°C in the base electrolyte, ~1M $SO_4^=$, having different pHs. The corrosion potential of Fe decreased linearly with increasing pH from 0.5 to 10 pH, it was relatively unchanged between pHs 10 and 12, but the potential decreased sharply at pH 13, see Figure 5. When sulfide was present in the solutions the corrosion potential at any pH was slightly below the original (sulfide free solution) potential, otherwise the effect of pH was similar to that described above. The active peak current decreased gradually with an increase in the pH but dropped suddenly to low values at pH > 11, see Figure 6. The behavior of Fe with respect to the minimum passive current density was different. The minimum passive current density increased, first gradually between 0.5 and 6 pH, then rapidly from 6 to 11 pH, and finally dropped for pH > 11, see Figure 7. It is clear that at 25°C in the active state of Fe acid

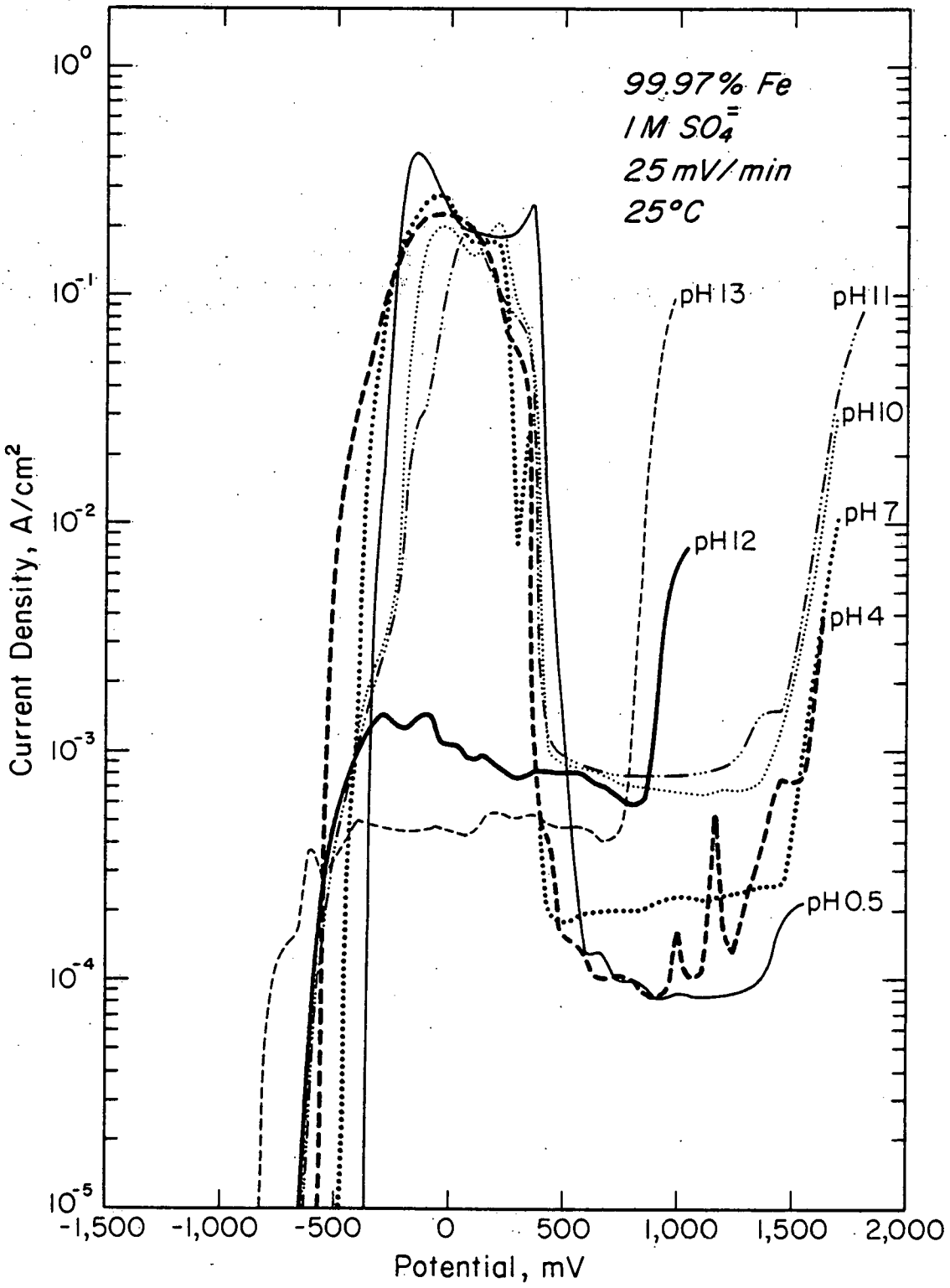

Figure 1 The effect of pH on the polarization behavior of 99.97% iron in 1M $SO_4^=$ solutions at 25°C.

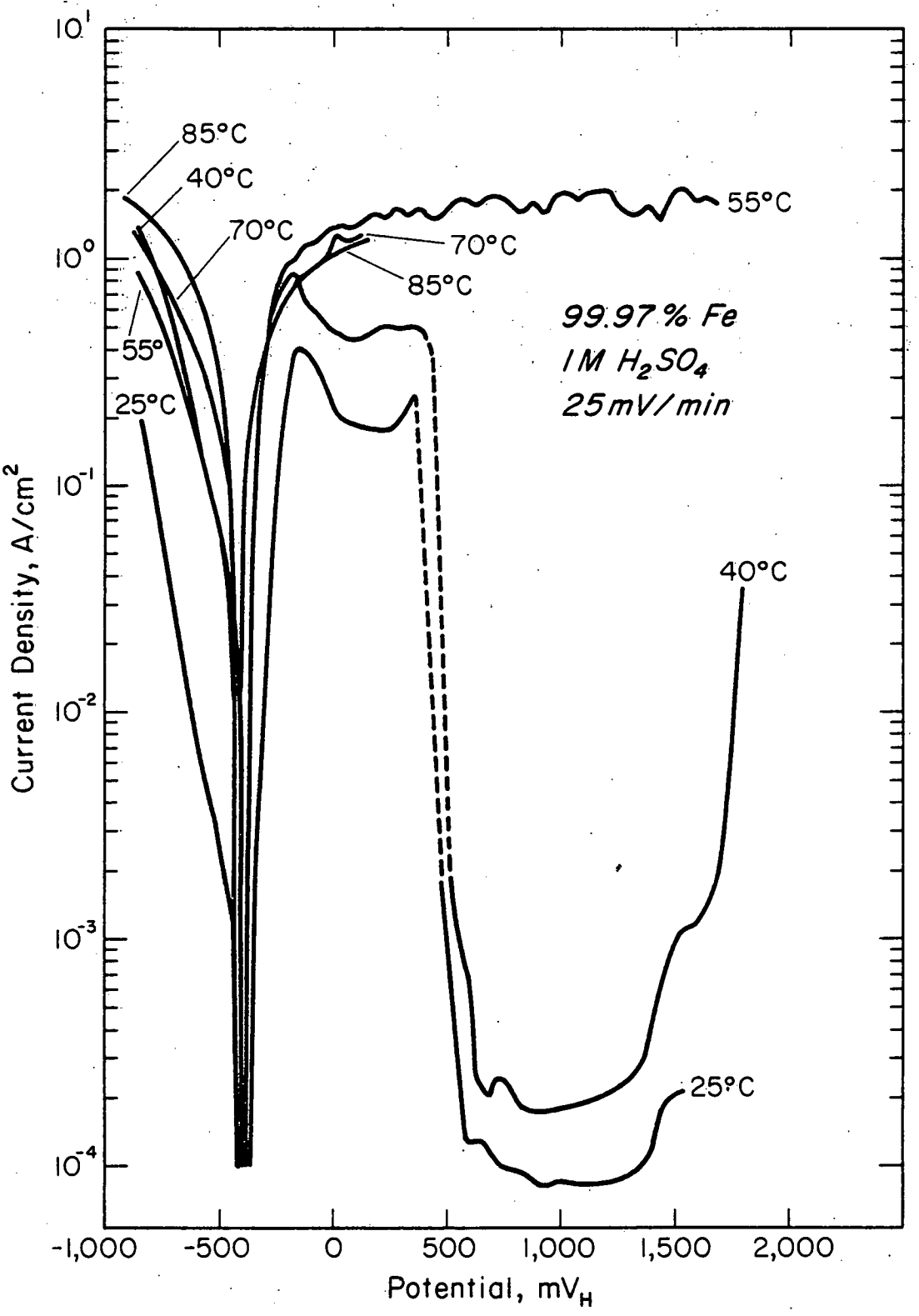

Figure 2 The effect of temperature on the polarization behavior of 99.97% iron in 1M H_2SO_4 solution.

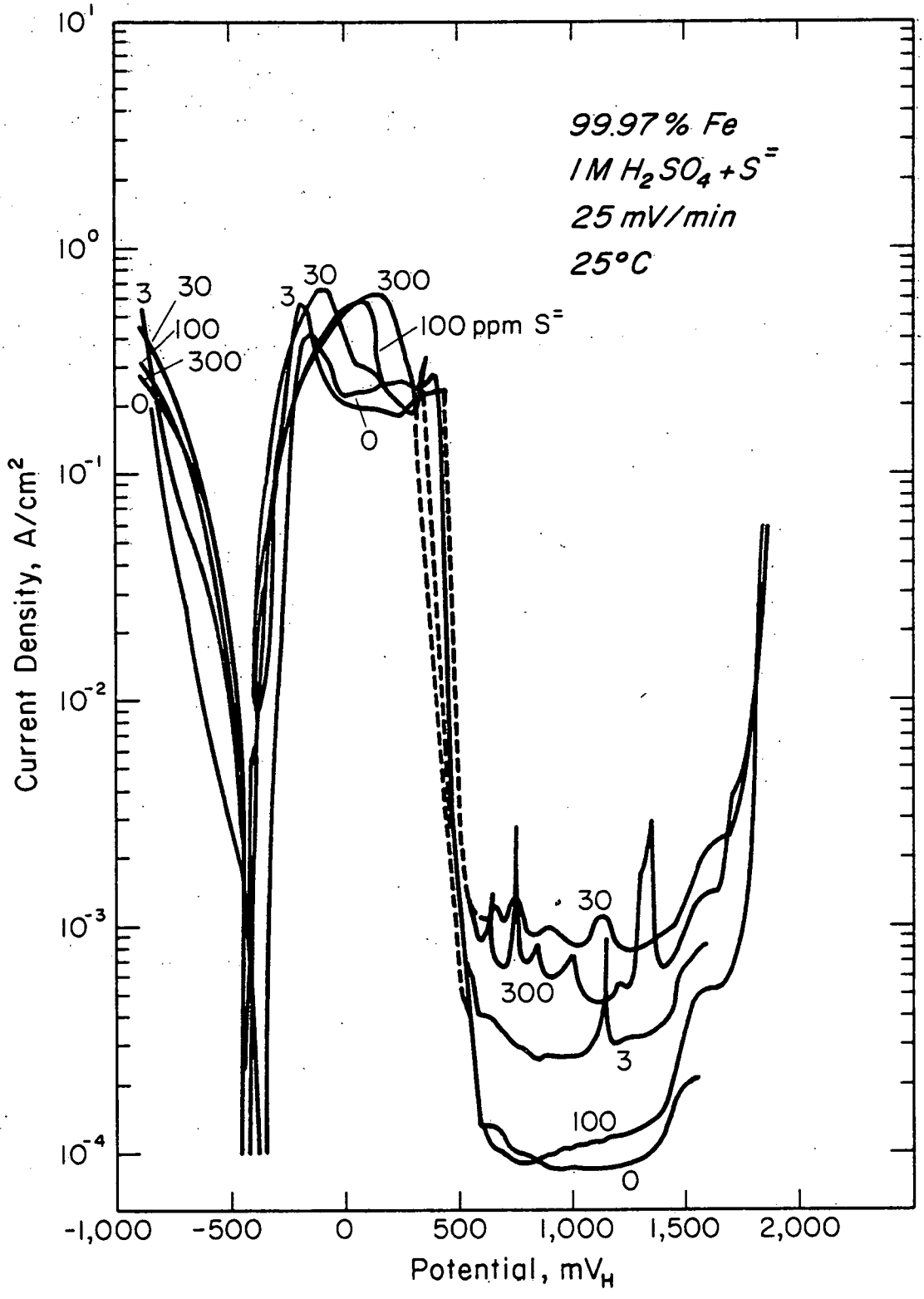

Figure 3 The effect of sulfide ions on the polarization behavior of 99.97% iron in 1M H_2SO_4 at 25°C.

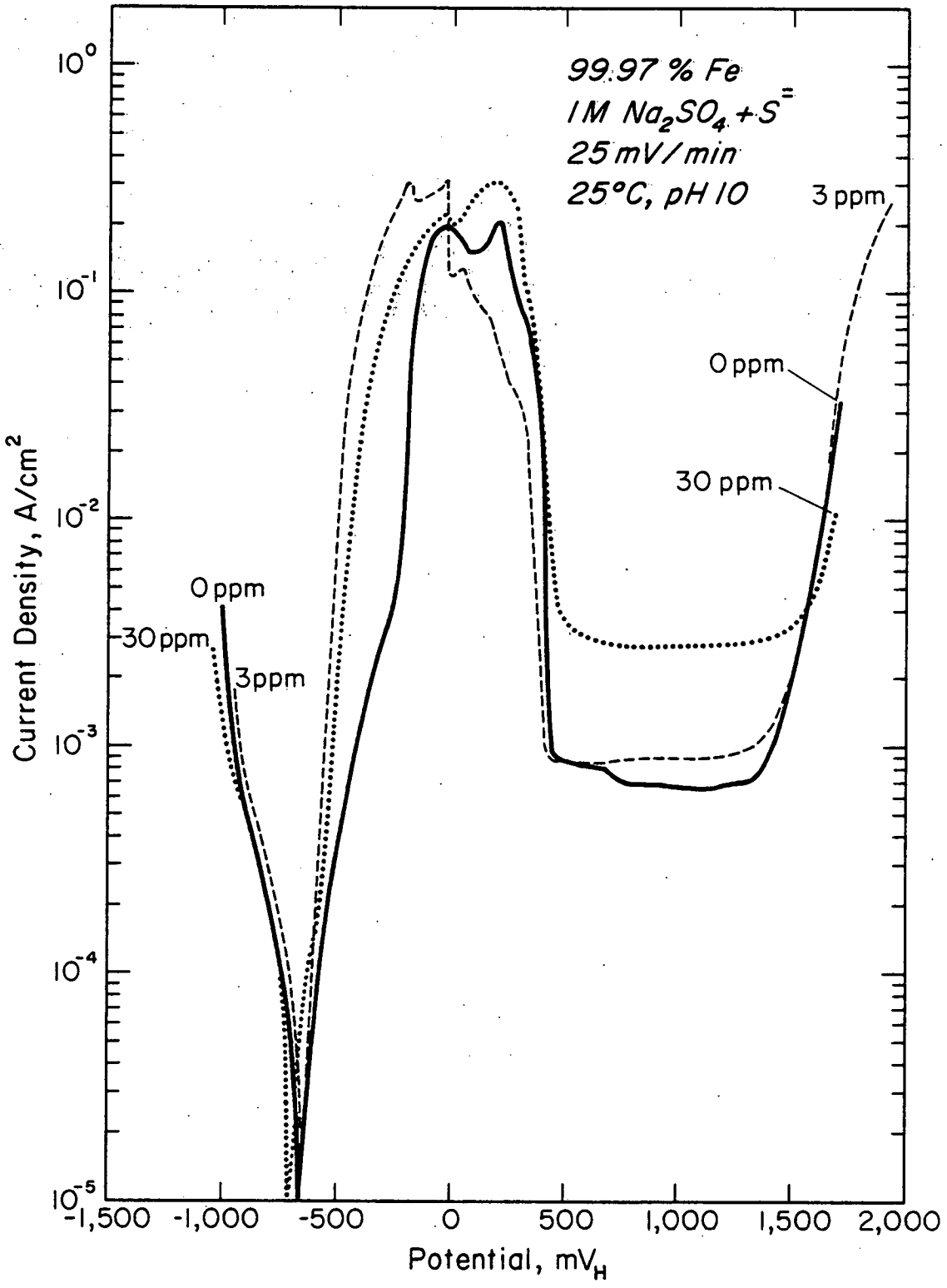

Figure 4 The effect of sulfide ions on the polarization behavior of 99.97% iron in 1M Na_2SO_4 solution at pH 10.0 and 25°C.

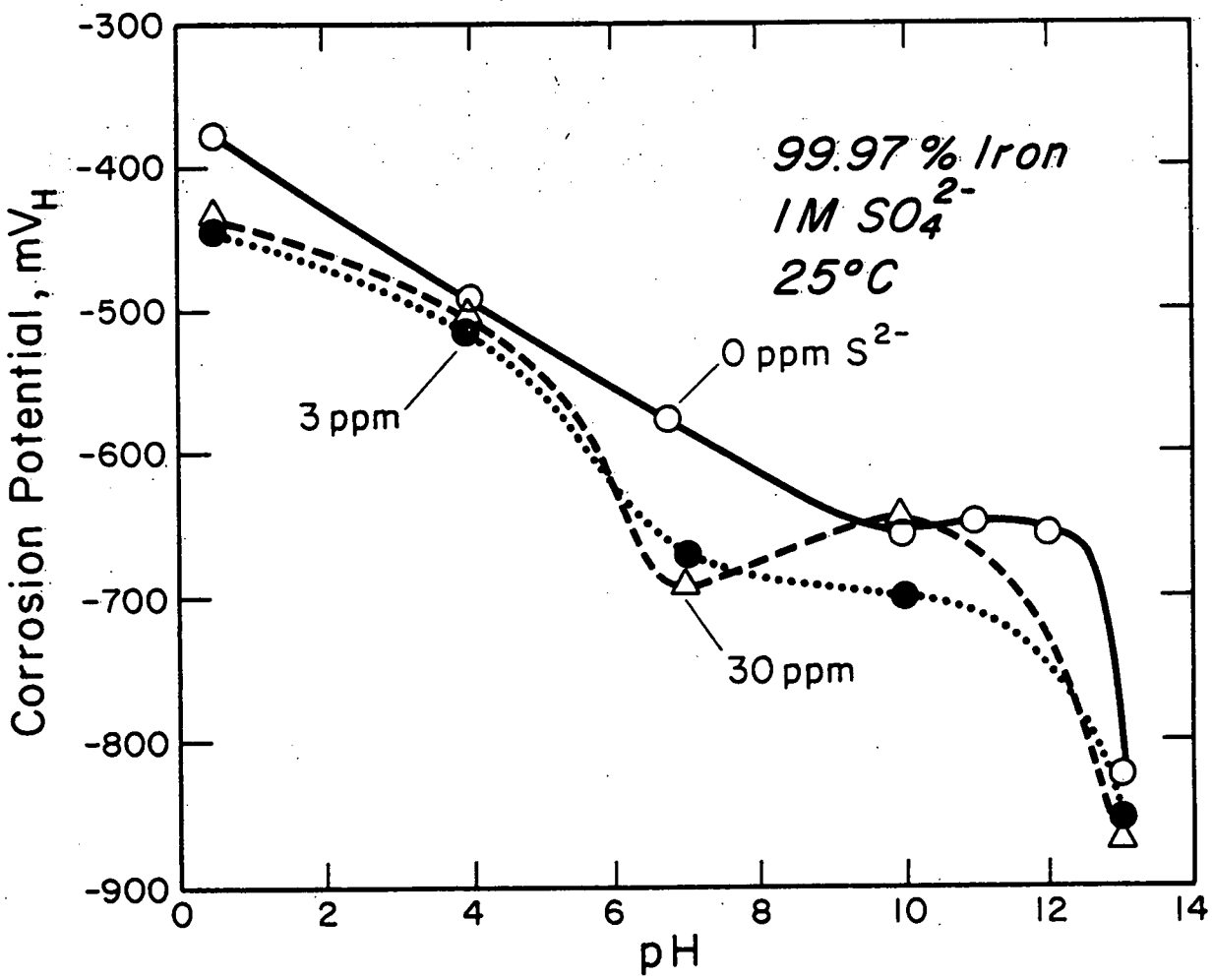

Figure 5 The effect of pH on the corrosion potential of 99.97% iron in 1M $SO_4^{=}$ solutions at 25°C in the absence and the presence of sulfide ions.

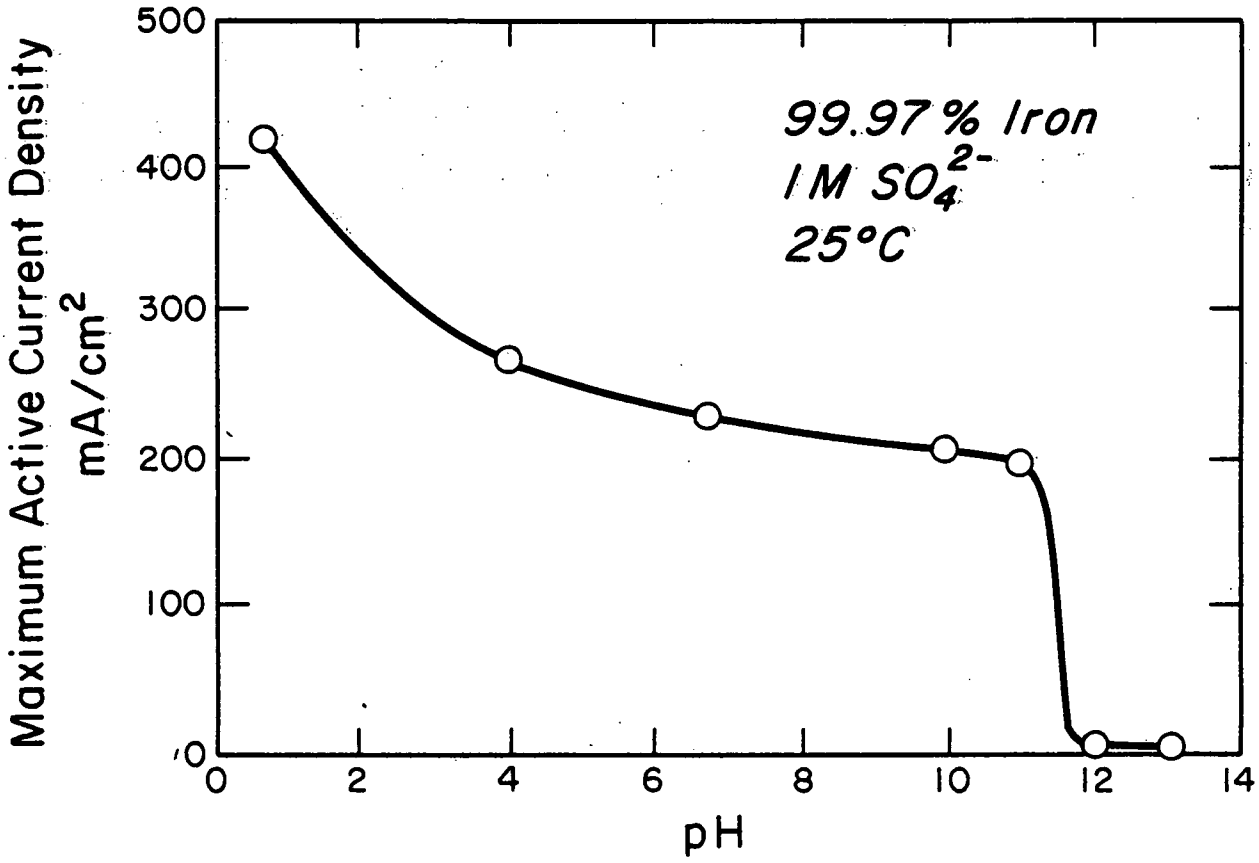

Figure 6 The effect of pH on the active peak current density of 99.97% iron in 1M $SO_4^=$ solutions at 25°C.

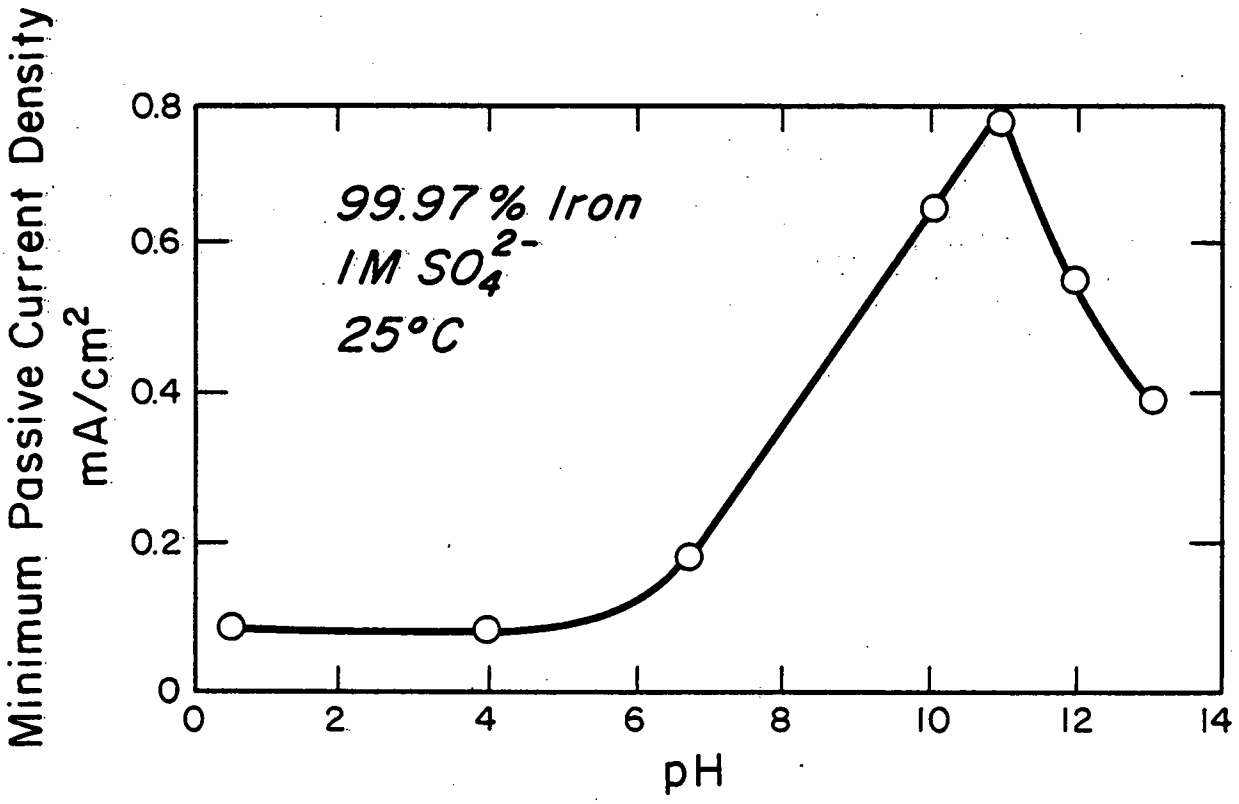

Figure 7 The effect of pH on the minimum passive current density of 99.97% iron in 1M $SO_4^=$ solutions at 25°C.

solutions are more corrosive than neutral or alkaline solutions. Whereas in the passive state acid solutions offer better protection than neutral and alkaline solutions.

The effect of temperature on the polarization behavior of Fe in sulfide free acid solution is shown in Figure 2. As the temperature increased the active current increased, but it reached an almost limiting value at 55°C. At 25°C Fe passivates in this solution with a current density which is 4 orders of magnitude less than the active peak value. However, no such passivation was observed at 55 to 85°C. The passivity of iron was completely destroyed at temperatures above 40°C.

The effect of sulfide ion on Fe in acid solution is shown in Figure 3. The active peak current increased with increasing sulfide concentration from 0 to 30 ppm. No further increase in current was observed with either 100 or 300 ppm Na_2S addition. However, the critical potential for passivation increased continuously with 0 to 300 ppm sulfide additions. In the passive region the current increased with sulfide additions but without a regular pattern. Considerable noise in the current recordings in the presence of sulfide suggests unstable films with pitting tendency in the passive region. In the acid solutions the solubility of H_2S is limited and probably because of this no significant trend in the current densities have been observed above 30 ppm.

In the alkaline solution of pH 10 the effect of $S^=$ on the active peak current of Fe is similar to that in acid solution, see Figure 4. However, in the passive region, the current increased with increasing $S^=$ ion concentration, similar to that in acid solution, but no tendency towards pitting was observed. In a still more alkaline solution of pH 13 the polarization curves in the presence or absence of $S^=$ ions had a general shape similar to that in Figure 4 for pH 10 solution.

Discussion and Conclusion

The potential/pH equilibrium diagram of Fe-S-H_2O system has been constructed by Biernat and Robins (1) in the temperature range 25 - 300 °C. According to their diagrams α - FeS or FeS_2 is to be expected on Fe electrode over the entire pH range 1 to 14 at 25°C. Horvath and Hackl (2) had developed similar diagram for this sytem at 25°C earlier. Later authors have also shown by potential decay techniques that the observed potential arrests in the pH range 1.1 to 7.4 correspond well with the theoretically calculated values. At higher anodic potentials FeS_2 oxidizes to Fe_3O_4. The above authors, however, have not commented on the passivating properties of the sulfide films.

In a recent paper Shoesmith et al (3) have shown that in the pH range 6.5 to 10 when sulfide is present in the solutions, the oxide growth on iron is inhibited which otherwise is formed in sulfide free solution. According to these authors at high anodic potentials breakdown of passivity occurs with the formation of sodium ferric sulfide. Further oxidation of this sulfide leads to the formation of elemental sulfur which causes repassivation of the surface. The concentration of sulfide in the solution determines the repassivation properties; excess sulfide leads to polysulfide formation and destruction of passivity.

The present results have not yet been analyzed in any detail with respect to thermodynamic stability of sulfides and oxides. Conclusions are withheld until further analyses.

REFERENCES

1. R. J. Biernat and R. G. Robbins, Electrochimica Acta, 17, 1261 (1972).
2. J. Horvath and L. Hackl , Corros. Sci., 5, 525 (1965).
3. D. W. Shoesmith, P. Taylor, M. G. Bailey, and B. Ikeda, Electrochimica Acta, to be published.

Task 3. Fundamental Electrochemical and Corrosion Studies in Aqueous Caustic Solutions at 25 to 150°C. U. Kim, A. K. Agrawal and R. W. Staehle.

Introduction

The aim of the present work was to find a reaction mechanism or mechanisms for the corrosion of nickel in its active and passive states in concentrated caustic solutions. It is hoped that when the corrosion mechanism is known it will be possible to predict long term corrosion rates from the developed rate equations. Potentiodynamic polarization curves give only instantaneous rates which may be quite different from the long term rates.

Experimental

Long term controlled potential coulometric experiments were done with Ni-270 in 10 N NaOH at 110°C and in 17.5 N NaOH at 130°C. These experiments were done in both the active and the passive potential regions of nickel in the above solutions.

Procedure. The nickel electrode, 12.5 mm x 6.2 mm dia., was polished to mirror finish with 600 grit SiC paper and cleaned with acetone and water prior to immersion in the deaerated test solution. The test solution was deaerated with purified (99.998% Ar minimum) argon and heated to the desired temperature with heating tapes around the Teflon cell. The cell capacity was ∿ 600 ml and it was filled with 400 ml of the solution. An internal Hg/HgO/NaOH reference electrode was used for the potential measurements; the concentration of NaOH in the reference electrode was the same as the test solution. The counter electrode was a platinum basket of several interconnected ∿ 7 cm dia. platinum rings.

The specimen was cathodically treated at -1250 mV (Hg/HgO) for about 10 minutes to remove the air formed film, before applying the desired potential. The potential was controlled with a Princeton Applied Research potentiostat Model 173. After applying the potential, the resulting current was followed on a Hewlett-Packard strip chart recorder whereas the coulombic charge was read off a Princeton Applied Research digital coulometer Model 379.

Results

The response of current at different potentials in 10N NaOH at 110°C is shown as a function of time in Figures 1 to 3. The results in Figure 1 are for potentials below the passivation potential, in Figure 2 for the active to passive transition region, and in Figure 3 for the passive potential region. Various potential regions can be identified from Figure 4, where the polarization curves of Ni in the 10 N NaOH are given at three different scan rates 0.5, 5.0 and 50 mV/sec. The general features of the current decay curves in Figures 1 to 3 are: 1) a current transient occurs when the potential is switched from the initial cathodic value to an anodic value (this transient due to its fast response, $< 10^{-1}$ min, was not resolveable on the recorder and therefore it is not shown in Figures 1 to 3), the transient peak current was high, $\sim$ 1 mA/cm^2 or more, in all cases; 2) the current after the transient peak decays to an arrest point; 3) thereafter the current rises to another peak value; 4) the current falls again to a negligibly small value; and finally 5) the current becomes cathodic, whose magnitude, irrespective of the applied potential is in the range $\sim$ 1 μA/cm^2.

The arrest time, τ_a, and the second peak time τ_p, as well as the respective current values i_a, and i_p are strongly dependent upon the applied potential. Both the τ_a and τ_p decreased as the potential was made more

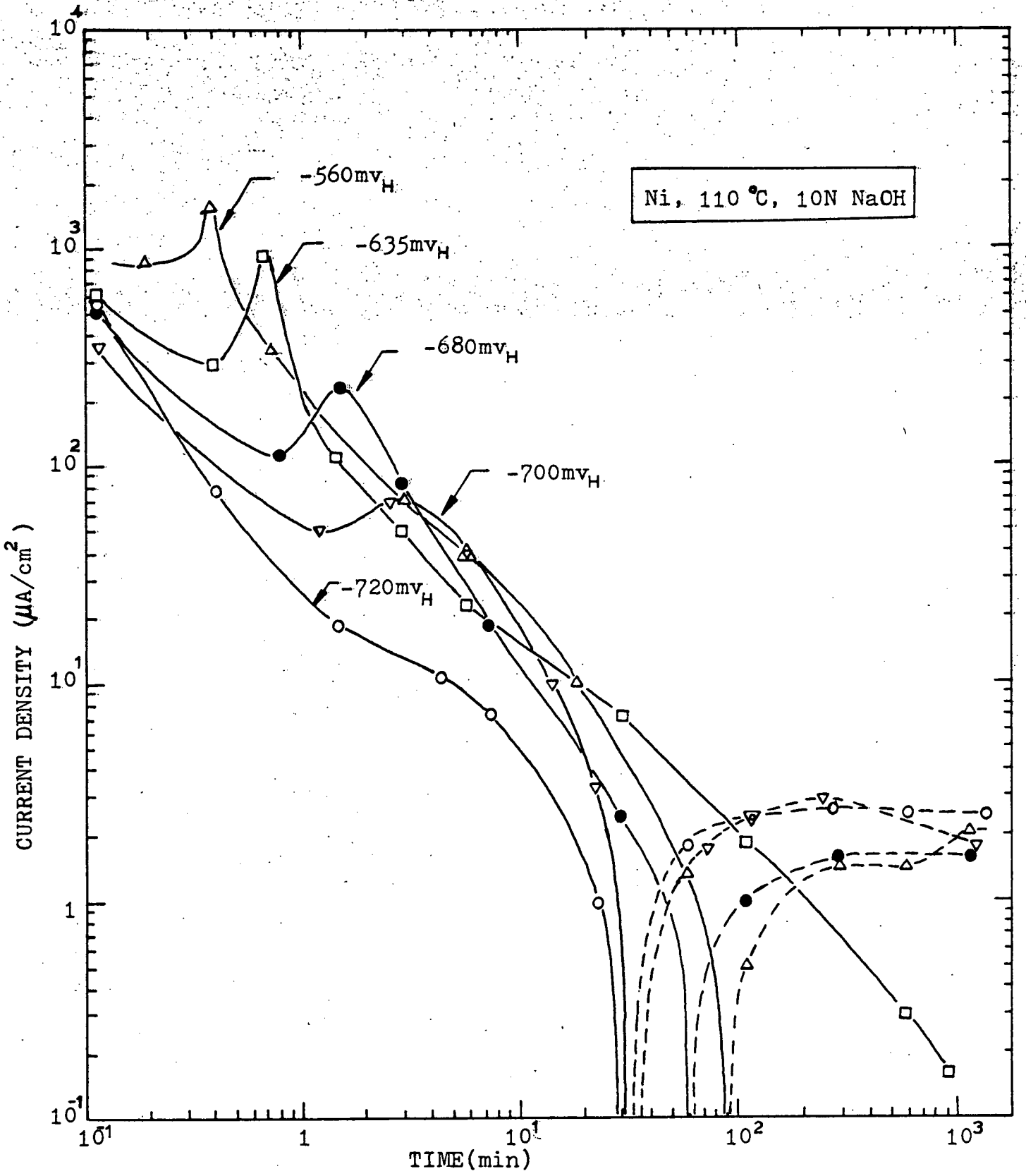

Figure 1 Current density vs. time at different potentials below the passivation potential for Ni in 10N NaOH at 110°C.

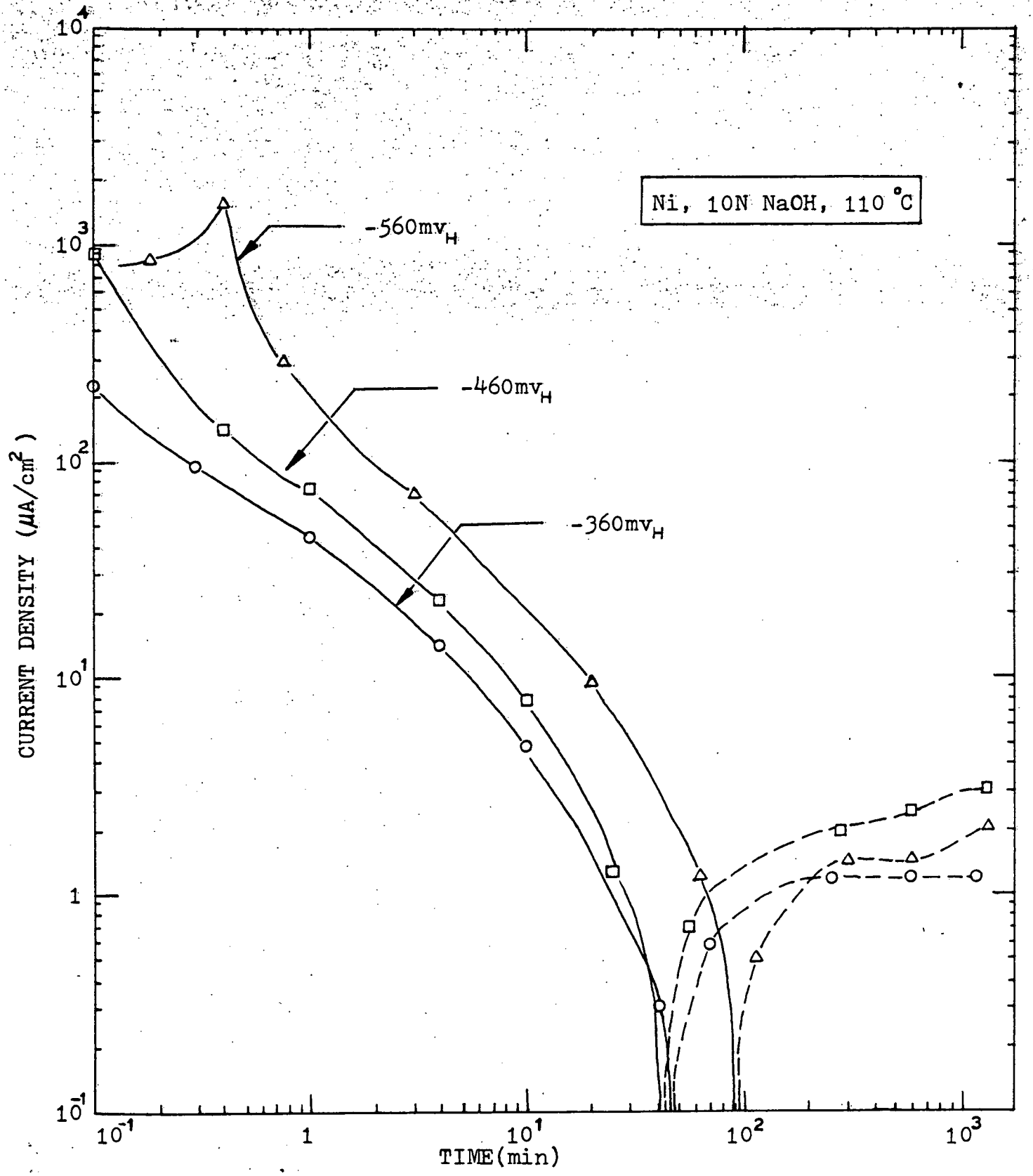

Figure 2 Current density vs. time at different potentials in the active to passive transition region for Ni in 10N NaOH at 110°C.

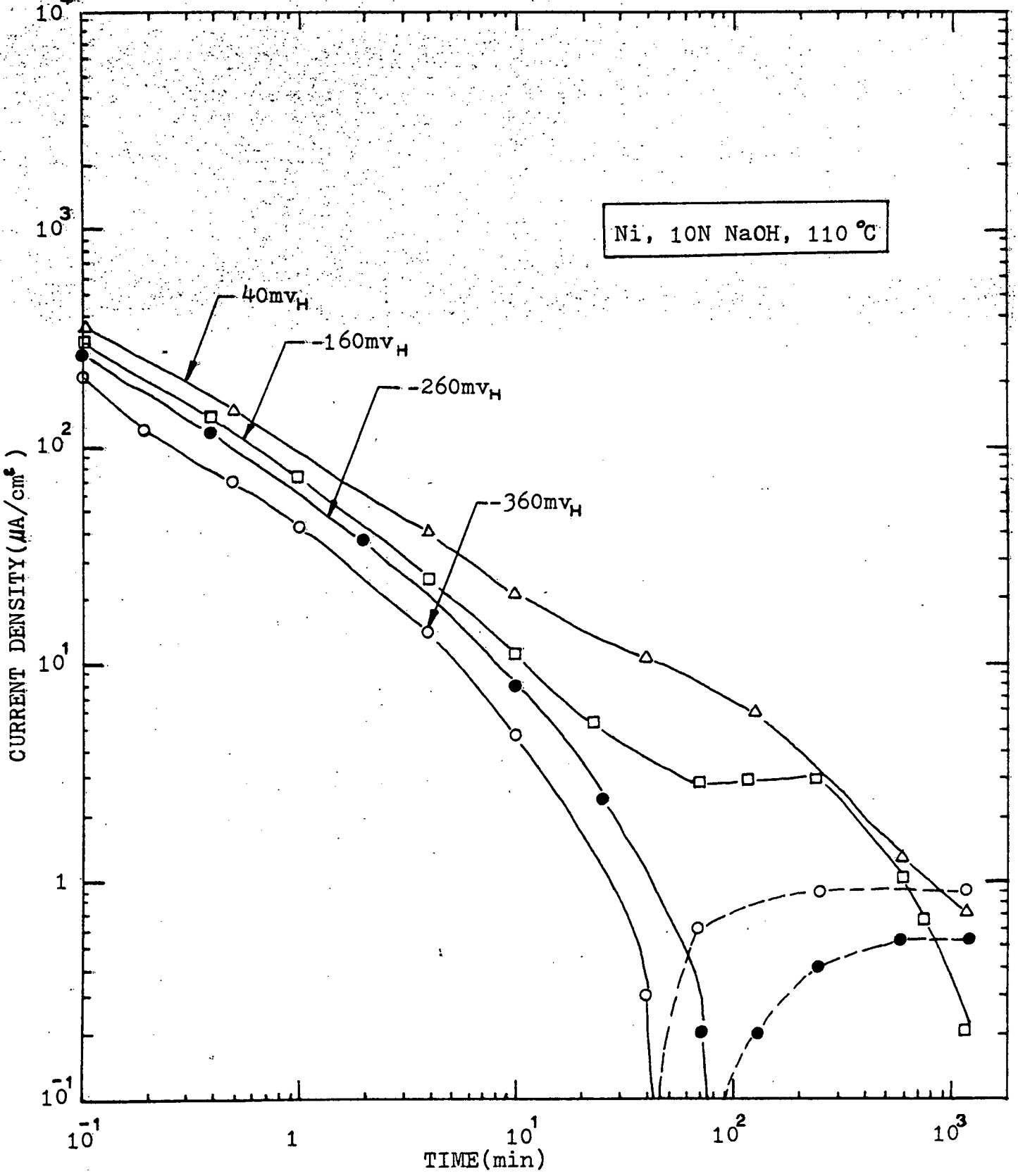

Figure 3 Current density vs. time at different potentials in the passive region for Ni in 10N NaOH at 110°C.

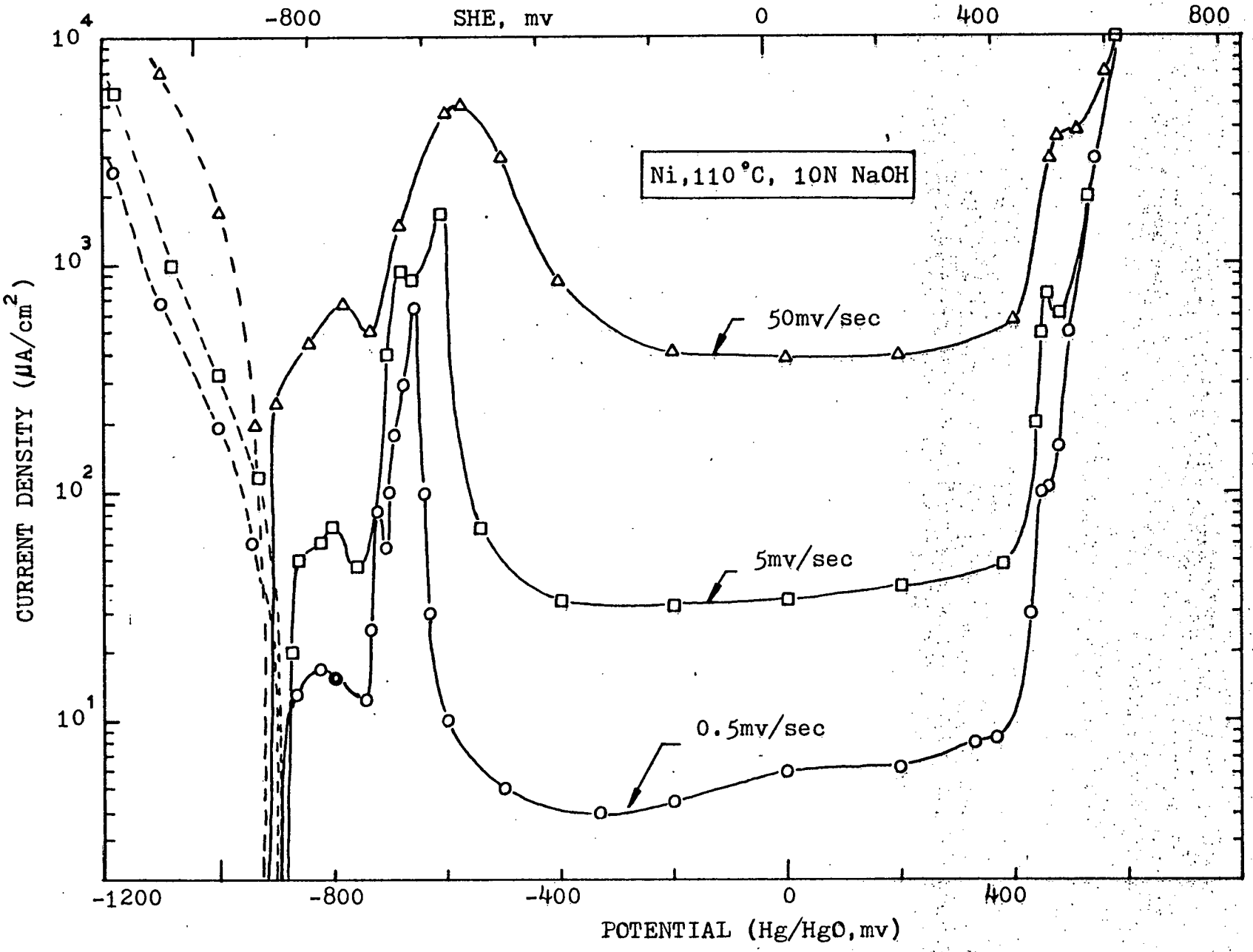

Figure 4 Cathodic and anodic polarization behavior of Ni in 10N NaOH at 110°C at different scan rates.

anodic, Figure 1. At high anodic potentials τ_a and τ_p were so small that these could not be measured, because of the slow response of the recorder. The arrest current and the peak current, on the other hand, both increased with the increasing potential. The decay of current after τ_p is logarithmic at all potentials, as shown for several potentials in Figure 5.

The response of current in 17.5 N NaOH at 130°C was similar to that described above. Some typical results for the short range decay are shown in Figure 6. In Figure 7 the total anodic change Q_T passed after stepping the potential and up to the peak time τ_p is plotted against τ_p for different potentials. A straight line relationahip is seen between the Q_T and τ_p, the slope of the line $\Delta Q_T/\Delta\tau_p$ is 0.39 mC/cm^2 sec. The line does not pass through Q_T=0 when it is extrapolated to τ_p=0, it intercepts at Q_T≈80 mC/cm^2. The curve in Figure 7 suggests that between time zero and time τ_p at least two processes are operating which contribute to the total charge Q_T. The first of the processes which contributes to zero time charge, Q_T° = 80, is potential independent. Whereas the second process is potential dependent, however, the rate of the process, $dQ_T/d\tau$, is not dependent upon the potential.

Solution analyses by atomic absorption spectrophotometer for dissolved Ni after each controlled potential experiment showed no enrichment of Ni in the caustic solution. Any Ni dissolved from the specimen during the test appears to have reprecipitated on the specimen surface as nickel oxide. In practically every case visual examination of the specimen after the tests showed a nonuniform green film on the surface. The results of visual examination are given in Table I. The composition of the precipitated oxide has not yet been determined.

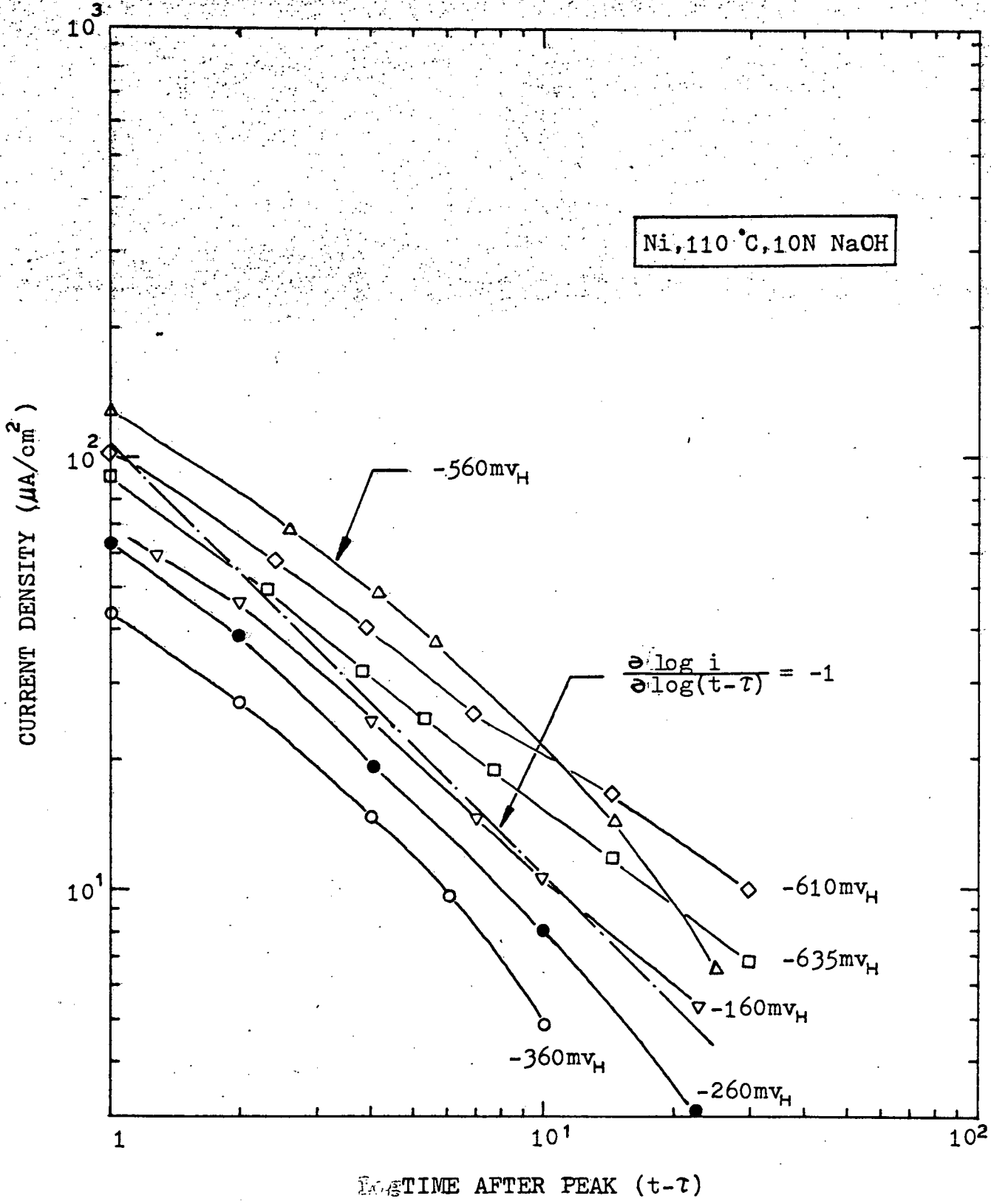

Figure 5 Current response after the peak time at different potentials for Ni in 10N NaOH at 110°C.

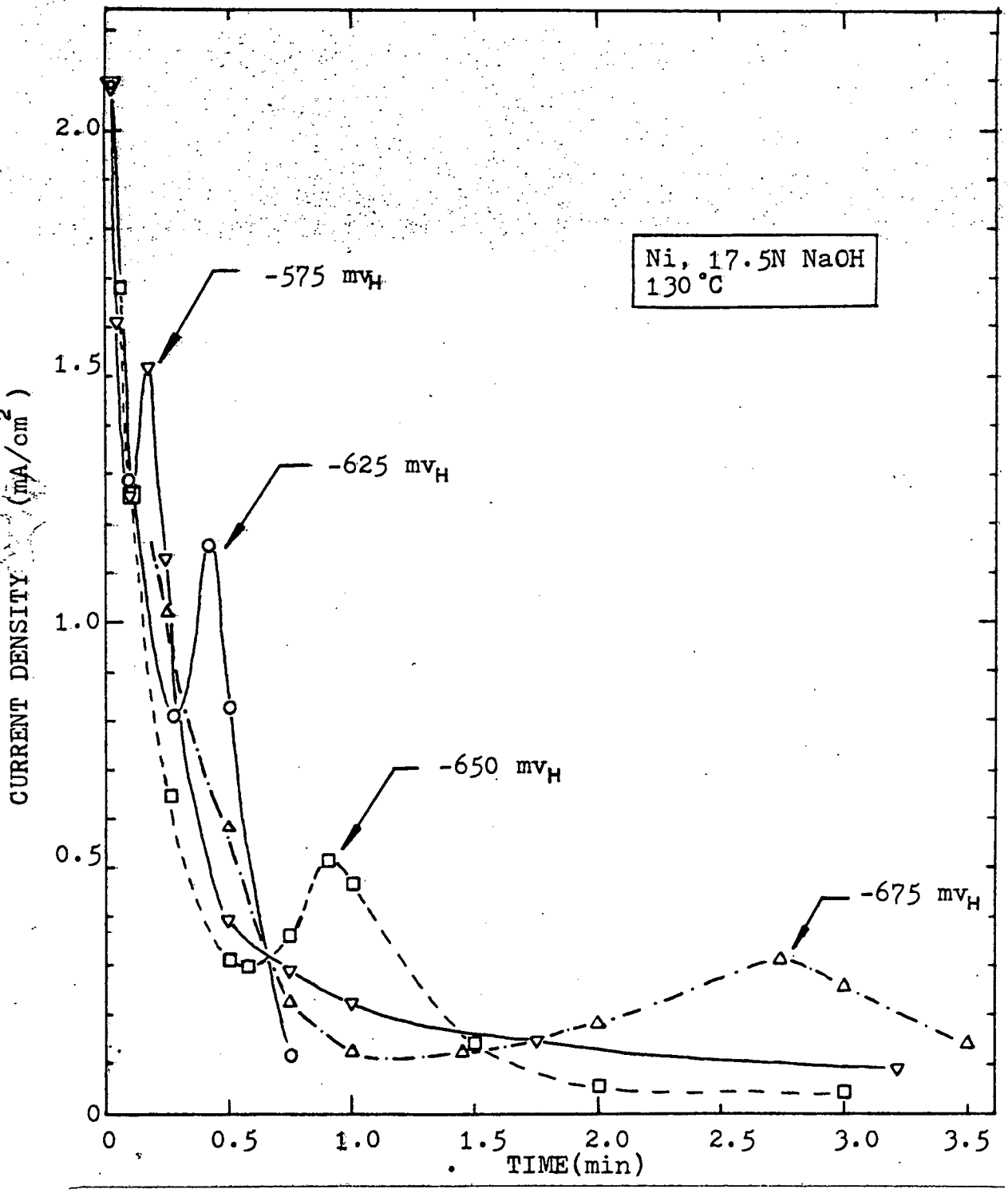

Figure 6 Current density vs. time at different potentials for Ni in 17.5N NaOH at 130°C.

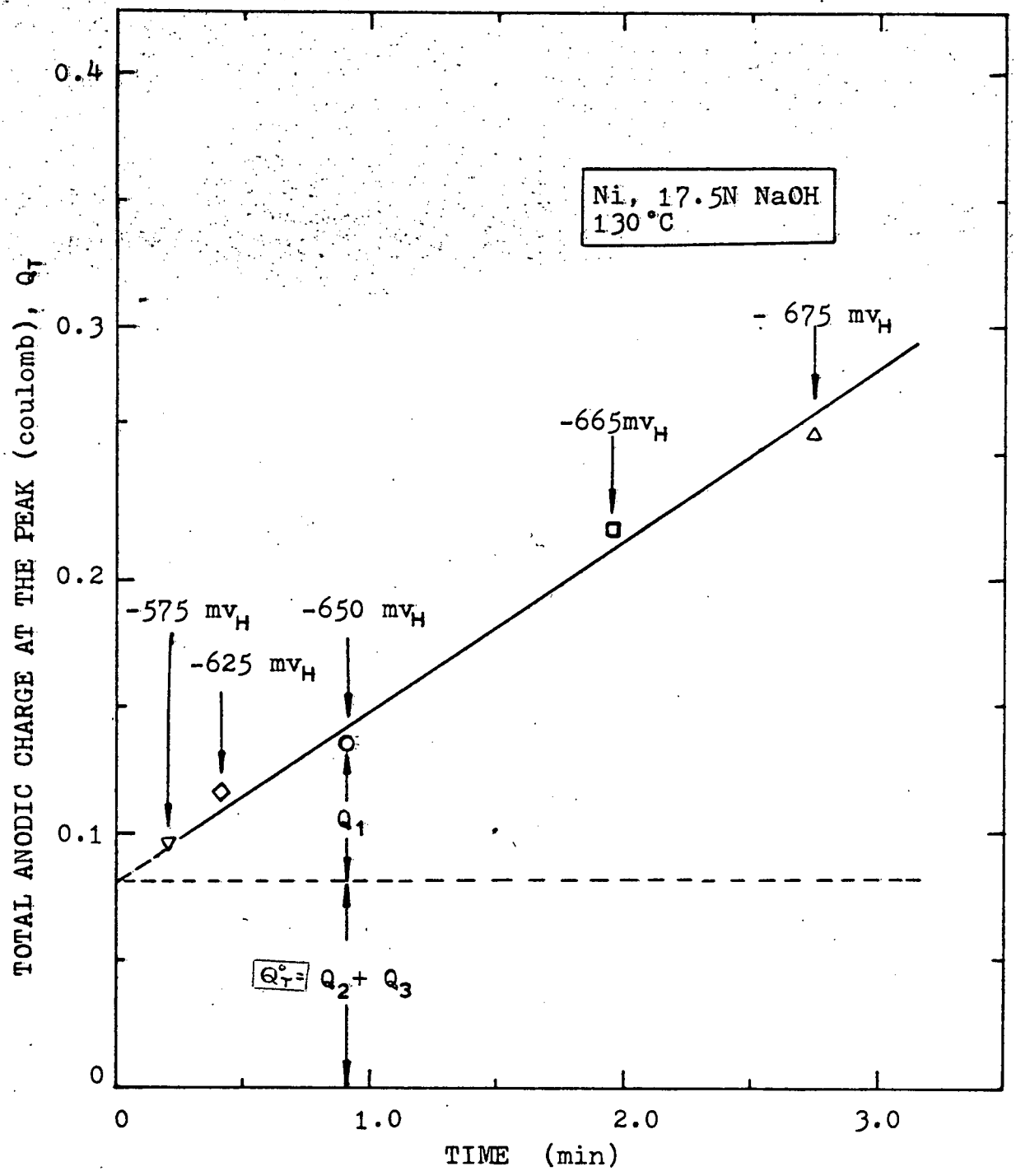

Figure 7 Total anodic charge at the peak vs. peak time at different potentials for Ni in 17.5N NaOH at 130°C.

Table I

Surface appearance of the Ni electrode after 20 hours exposure at various potentials in 10N NaOH at 110°C.

Potential mV_H	Surface Appearance
- 760	No change in brightness and color
- 720	Dull surface
- 700	Greenish film
- 680	Green film
- 635	Green Film
- 610	Green Film
- 560	Green Film
- 360	Light green film
- 160	Light green film

Discussion

The current response of Ni electrode at different potentials in caustic solutions is almost similar to that of Fe in neutral (1, 2) and alkaline (3) solutions. The logarithmic decay of current (after the second peak) with slope d log i/dt = -1 for film growth on Fe has been reported by Nagayama and Cohen (1, 2) and also by Asakura and Nobe (3). These authors, however, have not described the details of the electrode behavior between time zero and the time to second peak; this peak in iron appears to be less prominent than that in nickel.

Bockris et al (4) have described a dissolution-precipitation model of film growth for the passivation of Ni in acid solutions. According to this model the film growth starts on the electrode only after an induction time, τ, has elapsed. On applying an anodic potential, the metal dissolves and the metal ion concentration builds up at the metal-solution interface until the saturation is attained at τ, when the metal ions begin to precipitate on the metal surface causing passivation. During the concentration buildup at the interface some ions diffuse away into the bulk solution, and thus delay the induction time.

In our present case, the logarithmic film growth starts at time τ_p which is the induction time τ. The rate process responsible for the potential independent $dQ_T/d\tau$ in Figure 7 must be the diffusion process as will be proven below.

If we assume that $Q_T = Q_T^{\circ} + Q_{Diff}$, where Q_{Diff} is the charge associated with the amount W of metal ions which diffuse away from the metal-solution interface in time τ,

$$Q_{Diff} = \frac{nF}{M} \quad W$$

$$W = \int_0^{\tau} \text{Flux.} \frac{\text{Area}}{} dt$$

For diffusion through a cylindrical shell of length L with outer radius γ=b and inner radius γ=a having concentration $C_a = C_b + Kt$ at time t where $K = (C_s - C_b)/\tau$ and C_s is saturation concentration,

$$Q_{Diff} = \frac{nF}{M} \int_o^\tau \frac{D\,(C_a - C_b)}{\gamma \log b/a} \cdot 2\pi\gamma L \cdot dt$$

$$= \frac{nF}{M} \cdot \frac{2\pi LD}{\log b/a} \cdot \int_o^\tau (C_b + Kt - C_b)\, dt$$

$$= \frac{nF}{M} \cdot \frac{2\pi LD}{\log b/a} \cdot \frac{Cs - Cb}{2} \cdot \tau$$

$$= \text{constant} \cdot \tau$$

The relationship above suggests that Q_{Diff} is a linear function of τ for a cylindrical geometry. The results in Figure 7 show the linear relationship for the cylindrical specimen used in the present study.

Conclusion

Passivation of nickel in caustic solutions occurs after an incubation time which is dependent upon the applied potential. The incubation time is the time required for the nickel ions at the metal-solution interface to reach saturation concentration, whereupon oxide (hydroxide) precipitation occurs. The film growth after incubation follows a logarithmic kinetics. The dissolution-precipitation model of Bockris *et al* for Ni in acid solutions appears to be also applicable to caustic solutions.

REFERENCES

1. M. Nagayama and M. Cohen, Electrochem. Soc. J., 109, 781 (1962).
2. M. Nagayama and M. Cohen, Electorchem. Soc. J., 110, 670 (1963).
3. S. Asakura and K. Nobe, Electrochem. Soc. J., 118, 536 (1971).
4. J. O'M. Bockris, A. K. N. Reddy and B. Rao, Electrochem. Soc. J., 113, 1133 (1966).